

SOURCE  
DATATRANSPARENT  
PROCESS

# *Alu* element-containing RNAs maintain nucleolar structure and function

Maiwen Caudron-Herger<sup>1,\*</sup>, Teresa Pankert<sup>1</sup>, Jeanette Seiler<sup>2</sup>, Attila Németh<sup>3</sup>, Renate Voit<sup>2</sup>, Ingrid Grummt<sup>2</sup> & Karsten Rippe<sup>1,\*\*</sup>

## Abstract

Non-coding RNAs play a key role in organizing the nucleus into functional subcompartments. By combining fluorescence microscopy and RNA deep-sequencing-based analysis, we found that RNA polymerase II transcripts originating from intronic *Alu* elements (*alu*RNAs) were enriched in the nucleolus. Antisense-oligo-mediated depletion of *alu*RNAs or drug-induced inhibition of RNA polymerase II activity disrupted nucleolar structure and impaired RNA polymerase I-dependent transcription of rRNA genes. In contrast, overexpression of a prototypic *alu*RNA sequence increased both nucleolus size and levels of pre-rRNA, suggesting a functional link between *alu*RNA, nucleolus integrity and pre-rRNA synthesis. Furthermore, we show that *alu*RNAs interact with nucleolin and target ectopic genomic loci to the nucleolus. Our study suggests an *alu*RNA-based mechanism that links RNA polymerase I and II activities and modulates nucleolar structure and rRNA production.

**Keywords** *Alu* repeat-containing RNA; nucleolus structure and function; RNA-dependent phase separation

**Subject Categories** Chromatin, Epigenetics, Genomics & Functional Genomics; Transcription; RNA Biology

**DOI** 10.15252/embj.201591458 | Received 6 March 2015 | Revised 25 August 2015 | Accepted 31 August 2015 | Published online 13 October 2015

**The EMBO Journal (2015) 34: 2758–2774**

See also: **M Carmo-Fonseca** (November 2015)

## Introduction

Non-coding RNAs (ncRNAs) regulate a diverse set of nuclear activities and shape nuclear organization as an architectural factor (Caudron-Herger & Rippe, 2012; Batista & Chang, 2013; Mercer & Mattick, 2013; Bergmann & Spector, 2014). They are involved in the formation of nuclear bodies (Mao *et al.*, 2011; Shevtsov & Dundr, 2011), establish active or repressive chromatin states (Wong *et al.*, 2007; Deng *et al.*, 2009; Caudron-Herger *et al.*, 2011; Yang *et al.*, 2011) and regulate gene expression (Yao *et al.*, 2010;

Mercer & Mattick, 2013; Yang *et al.*, 2013; Bergmann & Spector, 2014).

The nucleolus is an exemplary case for the complex network between structure and function, demonstrating how RNA-dependent spatial organization affects transcriptional activity (Pederson, 1998; Carmo-Fonseca *et al.*, 2000; Olson *et al.*, 2000; Boisvert *et al.*, 2007; McKeown & Shaw, 2009). The nucleolus is highly sensitive to cellular stress, and environmental cues dynamically regulate its structure and activity (Rubbi & Milner, 2003; Olson, 2004; Sirri *et al.*, 2008; Boulon *et al.*, 2010). An important role for RNA in this process can be inferred from experiments that perturb transcription. Although RNA polymerase I (Pol I) transcribes nucleolar rRNA genes (rDNAs), inhibition of RNA polymerase II (Pol II) by  $\alpha$ -amanitin, 5,6-dichloro-1-beta-D-ribofuranosylbenzimidazole (DRB) or roscovitine (Chafin *et al.*, 1995; Sirri *et al.*, 2002) leads to disintegration of nucleoli (Granick, 1975; Scheer *et al.*, 1984; Chafin *et al.*, 1995; Haaf & Ward, 1996; Sirri *et al.*, 2002; Burger *et al.*, 2010). Inhibition of Pol II transcription is accompanied by down-regulation of rRNA synthesis, indicating that yet-to-be-identified Pol II transcripts may regulate nucleolar organization and Pol I transcriptional activity (David-Pfeuty *et al.*, 2001).

Transcripts from the intergenic spacer that separates individual rRNA genes have been linked to epigenetic regulation of Pol I transcription (Mayer *et al.*, 2006), to sequestering proteins in the nucleolus upon cellular stress (Audas *et al.*, 2012) and to remodeling of the nucleolus (Jacob *et al.*, 2013). A recent study identified Pol II transcripts in antisense orientation to the pre-rRNA coding region, which recruit the histone methyltransferase SUV4-20H2 to rRNA genes to induce histone H4 lysine 20 trimethylation and chromatin compaction in growth-arrested cells (Bierhoff *et al.*, 2014). In addition, novel functional transcripts originating from the intergenic spacer of rDNA repeats and synthesized by Pol I have been implicated in the nucleolar stress response to maintain cellular homeostasis (Audas *et al.*, 2012; Jacob *et al.*, 2012, 2013). Finally, the association of the NAD<sup>+</sup>-dependent deacetylase SIRT7 to nascent pre-rRNA stabilizes the interaction of SIRT7 with Pol I, being a prerequisite for SIRT7-dependent transcription activation (Chen *et al.*, 2013). However, a detailed analysis of the role of regulatory nucleolar transcripts for the structure and activity of the nucleolus is lacking.

1 Genome Organization & Function, German Cancer Research Center (DKFZ), Bioquant Center, Heidelberg, Germany

2 Molecular Biology of the Cell II, German Cancer Research Center, Heidelberg, Germany

3 Department of Biochemistry III, Biochemistry Center Regensburg, University of Regensburg, Regensburg, Germany

\*Corresponding author. Tel: +49 6221 5451373; E-mail: m.caudron@dkfz.de

\*\*Corresponding author. Tel: +49 6221 5451376; E-mail: karsten.rippe@dkfz.de

Here, we combined high-resolution fluorescence microscopy and RNA deep sequencing to address this issue. We found that Pol II transcripts originating from intronic *Alu* elements (*alu*RNAs) play an important role in the assembly and function of the nucleolus. *Alu* repeats are the most abundant repetitive elements of primates constituting more than 10% of the human genome (Batzer & Deininger, 2002). *Alu* transcripts are synthesized by both RNA polymerase III (Pol III) and II. “Free *Alu* RNAs”, that is, RNAs transcribed from *Alu* elements that are not embedded within genes, as well as the related 7SL RNA, are produced by Pol III using the internal promoter of *Alu* elements. In contrast, “embedded *Alu* RNAs” are localized within introns, transcribed by Pol II and spliced out from pre-mRNA during mRNA maturation (Deininger, 2011). *Alu* transcripts have been shown to regulate gene expression post-transcriptionally, being involved in alternative splicing (Singer *et al*, 2004), RNA editing (Mattick & Mehler, 2008) and translation efficiency (Capshaw *et al*, 2012; Fitzpatrick & Huang, 2012), but have not been linked to the functional organization of nuclear subcompartments. In the present study, we show that Pol II-dependent *alu*RNAs regulate nucleolar structure and rRNA synthesis via interaction with nucleolin (NCL), a major structural and multifunctional nucleolar protein with pivotal functions in ribosome biogenesis (Ginisty *et al*, 1999). Our results uncover a novel mechanism that links Pol I transcription levels with global Pol II activity via nuclear *alu*RNA production and suggest an *alu*RNA-dependent mechanism that preserves nucleolar structure and function.

## Results

### Functional nucleolus structure requires Pol II transcription

To address the response of nucleolar structure to the inhibition of transcription, we treated HeLa cells for 5 h with drugs that specifically inhibit each of the three polymerases (Fig 1A). Notably, a Pol II-specific structural phenotype was observed after inhibition of Pol II transcription by  $\alpha$ -amanitin (Weinmann & Roeder, 1974) or DRB (Fig 1A and Appendix Fig S1A). Nucleoli were disrupted into small domains, and rDNA was scattered throughout the nucleus. These observations suggest that active Pol II transcription is needed for the structural integrity of the nucleolus, although this nuclear compartment has very little apparent Pol II activity (Roeder & Rutter, 1970; Sirri *et al*, 2008). Drug-mediated perturbations of nucleolar structure correlated with a clearly impaired nucleolar function as revealed by strong reduction in pre-rRNA synthesis (Appendix Fig S1B and C) (David-Pfeuty *et al*, 2001). Moreover, NCL, Pol I and the Pol I-specific transcription factor UBF became dispersed throughout the nucleoplasm after  $\alpha$ -amanitin treatment (Fig 1A and Appendix Fig S1D and E). In the following, we refer to this phenotype as nucleolar dispersion or dispersed nucleoli, which are characterized by the dissociation of nucleoli into small nucleolar domains and the loss of co-localization of the nucleolar components. These changes of nucleolar structure after Pol II inhibition were clearly different from those induced by treatment of cells with low doses of actinomycin D (AMD), which blocks Pol I transcription elongation and causes nucleolar segregation (Fig 1A), that is, condensation of rDNA in nucleolar caps (Reynolds *et al*, 1964). Moreover, efficient inhibition of Pol III transcription by ML-60218 (Wu *et al*, 2003; Di Ruscio *et al*,

2013) did not result in nucleolar dispersion (Fig 1A and Appendix Fig S1F). Likewise, treatment with cycloheximide for 5 h did not affect nucleolar structure, demonstrating that disruption of nucleoli after  $\alpha$ -amanitin treatment was not due to abrogation of protein synthesis (Appendix Fig S1G). Thus, the absence of a nucleolar dispersion phenotype after specific inhibition of Pol I, III or protein synthesis demonstrates that Pol II transcription is needed to maintain the structure of the nucleolus and the efficient production of pre-rRNA by Pol I.

### Nucleolar RNA partially rescues $\alpha$ -amanitin-mediated disruption of nucleoli

Our results obtained after  $\alpha$ -amanitin treatment do not distinguish whether Pol II transcription *per se* or Pol II transcripts are required for maintaining nucleolar structure. If Pol II transcripts stabilize nucleoli, Pol II transcripts should be present in nucleoli. To test this, we isolated RNA from purified nucleoli that were devoid of substantial contaminations by cytoplasmic or nucleoplasmic RNA (Appendix Fig S2). Small nucleolar RNAs (snoRNA) displayed strong enrichment in the nucleolar RNA fraction (Richard *et al*, 2003). In contrast MALAT1, a highly abundant ncRNA that localizes to nuclear speckles (Hutchinson *et al*, 2007), was absent as compared to total RNA and the nucleoplasmic fraction. Consistent with a small fraction of Cajal bodies being associated with nucleoli (Raska *et al*, 1990), Cajal body-specific RNAs (scaRNAs) were present in the nucleoplasmic and nucleolar fractions.

Next, we tested the capability of the purified nucleolar RNA to rescue the disrupted nucleolar phenotype observed upon the inhibition of Pol II transcription. As reported above,  $\alpha$ -amanitin treatment induced dispersion of nucleoli into smaller nucleolar domains. This process was quantified by a more than two-fold increase in their number from  $n = 3.3 \pm 0.3$  to  $n = 8.1 \pm 1.0$  with an average size of  $1.1 \pm 0.1 \mu\text{m}^2$  (Fig 1B). Microinjection of RNA from purified nucleoli but not from total RNA was capable of rescuing nucleolar perturbation caused by  $\alpha$ -amanitin treatment. As shown in Fig 1B, larger and fewer nucleolar domains ( $n = 4.7 \pm 0.4$  with an average size of  $2.3 \pm 0.3 \mu\text{m}^2$ ) were observed after microinjection of nucleolar RNA into  $\alpha$ -amanitin-treated HeLa cells. This indicates that the nucleolar RNA fraction contains RNA transcripts that counteract the  $\alpha$ -amanitin-mediated segregation of active nucleolus organizer regions.

### *Alu* element-containing Pol II transcripts are enriched in the nucleolus

To identify the RNA transcripts that stabilize nucleolar structure, we looked for transcripts that were specifically enriched in the nucleolar RNA fraction. We performed RNA-seq and a comparative bioinformatic analysis of data sets obtained from nucleolar and nucleoplasmic RNA fractions as well as total RNA. Nucleolar RNA was markedly enriched in reads mapping to “intronic-only” sequences, that is, sequences not associated with exonic parts of the corresponding primary transcripts (Appendix Table S1). The nucleolar “intronic-only” sequences were enriched in *Alu* repeat elements as compared to the total RNA or nucleoplasmic RNA fractions. We here refer to these *Alu* repeat-containing transcripts that are overrepresented in nucleolar RNA as *alu*RNAs. Generally, intron-encoded *alu*RNAs clustered into transcripts covering either

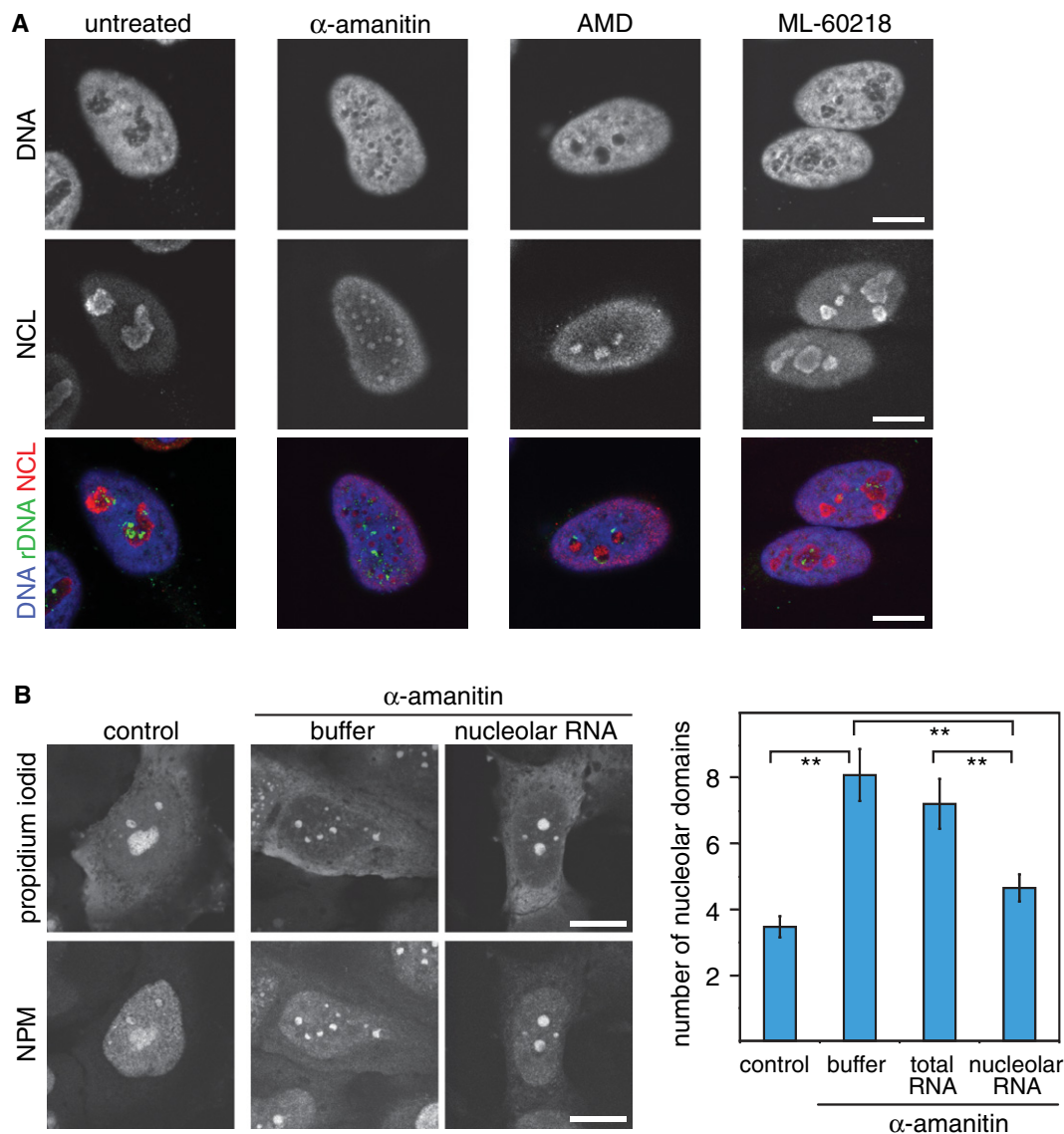


**Figure 1. Pol II transcription is essential for nucleolar structure and function.**

**A** Confocal laser scanning fluorescence microscopy (CLSM) images showing DNA staining (blue in the merged images), rDNA FISH (green) and NCL immunofluorescence (red) in untreated HeLa cells or in cells treated with  $\alpha$ -amanitin (50  $\mu$ g/ml), AMD (50 ng/ml) or the Pol III inhibitor ML-60218 (200  $\mu$ M) for 5 h.

**B** CLSM images of propidium iodide-stained RNA after microinjection of buffer or nucleolar RNA into  $\alpha$ -amanitin-treated HeLa cells. Nucleoli were visualized by immunofluorescence of nucleophosmin (NPM). The graph represents the average number of nucleolar domains ( $\pm$  95% CI) based on the analysis of 90, 87, 80 and 86 cells, respectively. \*\**P*-value < 0.01, *t*-test.

Data information: Scale bars, 10  $\mu$ m.

See also Appendix Figs S1 and S2.

the whole *Alu* sequence or only a truncated left (*aluRNA<sub>L</sub>*) or right (*aluRNA<sub>R</sub>*) arm in either forward or reverse orientation within the primary transcript (Fig 2A). In the total RNA fraction, most *aluRNAs* were found in long primary transcripts (> 2,000 nt) (Appendix Table S2). In the nucleolar RNA fraction, however, isolated *aluRNA* sequences lacking flanking sequences were markedly enriched and, on an average, about 100-fold more abundant than in total RNA or nucleoplasmic RNA (Fig 2B and C, Appendix Tables S2 and S3). The most abundant nucleolar *aluRNAs* were about 250 nt in length and corresponded to a

forward *aluRNA<sub>R</sub>* sequence that lacked the box A and box B element (Fig 2A and B, Appendix Figs S3 and S4). The level of most nucleolar *aluRNAs* was decreased after  $\alpha$ -amanitin treatment, whereas the inhibition of Pol III transcription did not affect the abundance of nucleolar *aluRNAs* (Fig 2D), confirming that Pol II synthesizes nucleolar *aluRNAs*.

To corroborate that *aluRNA* sequences were enriched in nucleoli, we conducted RNA FISH experiments with probes that hybridize to nucleolar *aluRNA* in forward or reverse orientation. The results confirmed that both types of *aluRNAs* accumulated in the

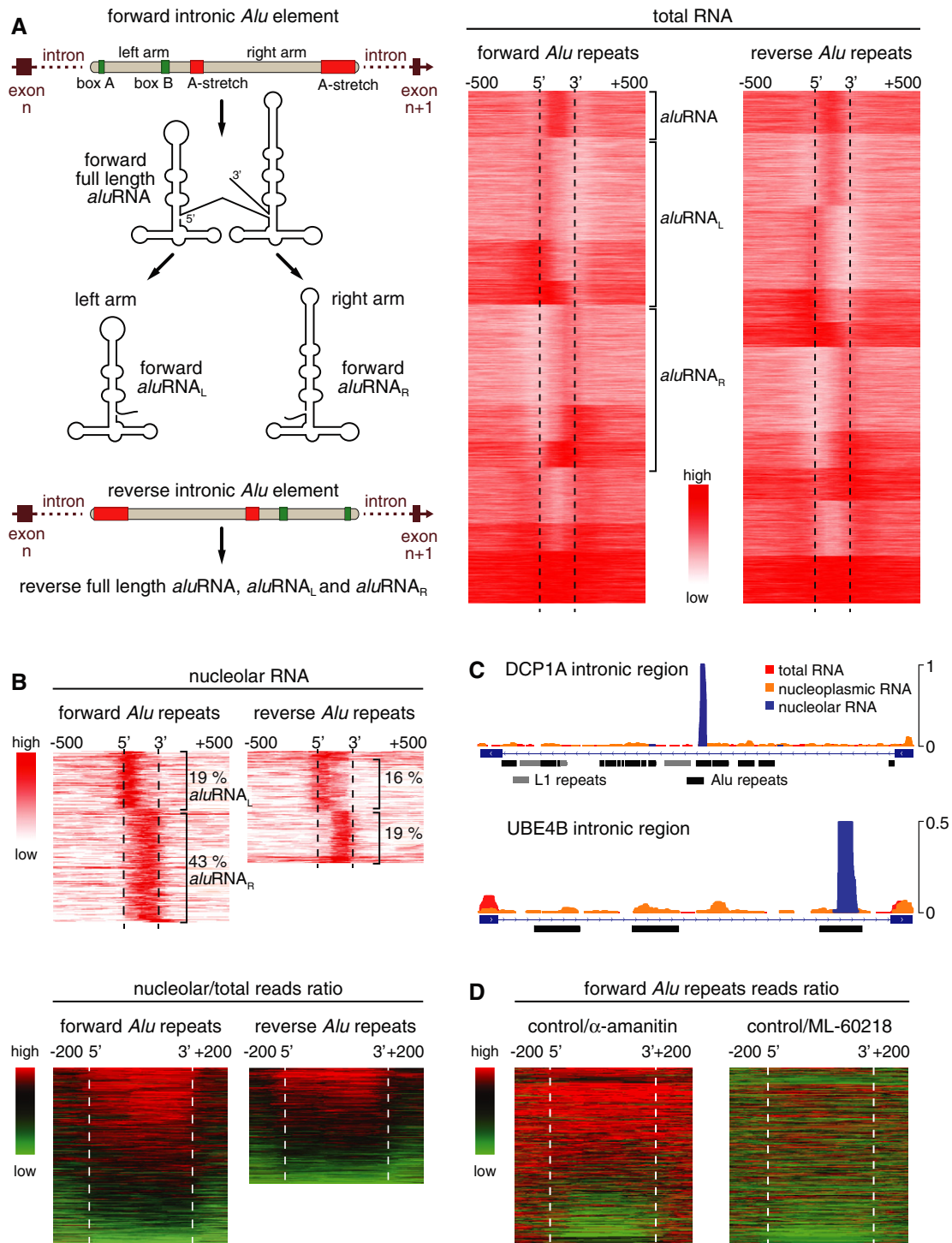


**Figure 2. Nucleolar RNA is enriched in specific intron-encoded *Alu*RNAs.**

A Left: Scheme illustrating the origin of forward or reverse intronic *Alu*RNA and processing into left arm *Alu*RNAs (*AluRNA<sub>L</sub>*) and right arm *Alu*RNAs (*AluRNA<sub>R</sub>*). Right: Heatmaps of read density of forward and reverse intronic *Alu* RNA species present in the total RNA sample.

B Top: Heatmaps of read density of intronic *Alu* repeats in the nucleolar RNA fraction. For each *Alu*RNA variant, the percentage over all transcribed intronic *Alu* repeats is indicated. Bottom: Ratio of nucleolar versus total RNA from higher (red) to lower (green) read density.

C View of nucleolus-enriched *Alu* elements exemplified at two genomic loci. Mapping of normalized reads from total (red), nucleoplasmic (orange) and nucleolar (blue) RNA to intron #5 of DCP1A and intron #22 of UBE4B.

D Heatmaps of total RNA read density ratios between untreated (control) and  $\alpha$ -amanitin- or ML-60218-treated HeLa cells.

See also Appendix Figs S3 and S4, Appendix Tables S2 and S3.

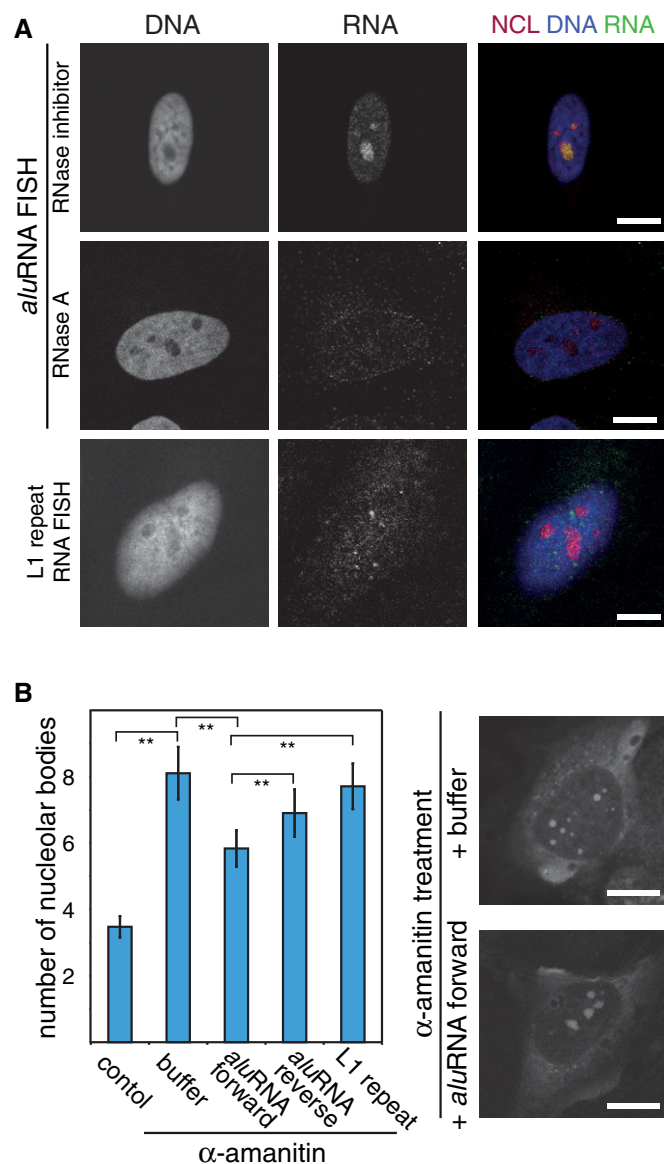


**Figure 3. *alu*RNA is localized to nucleoli and partially rescues  $\alpha$ -amanitin-induced nucleolar dispersion.**

**A** CLSM images showing nucleolar co-localization of NCL (immunofluorescence) with *alu*RNA (RNA FISH) but not with L1-repeat RNA. Cells were pre-treated *in situ* with RNase A or an RNase inhibitor. Nuclei were counterstained with DAPI. The signal intensity of nucleolar *alu*RNA was two-fold higher compared to nucleoplasmic signal ( $n = 92$ ,  $P$ -value  $< 0.05$ ,  $t$ -test).

**B** Graphs representing the average number of nucleolar bodies after microinjection of *in vitro* transcribed RNA into HeLa cells that were pre-treated with  $\alpha$ -amanitin (50  $\mu$ g/ml) for 5 h or left untreated (control) ( $\pm$  95% CI. \*\* $P$ -value  $< 0.01$ ,  $n = 90, 87, 86, 83$  or 86 cells, respectively). Representative CLSM images of propidium iodide-stained RNA are shown on the right side.

Data information: Scale bars, 10  $\mu$ m.

See also Appendix Fig S5, Appendix Table S4.

nucleoli (Fig 3A and Appendix Fig S5A–C). Furthermore, a Northern blot analysis of total RNA revealed the presence of *alu*RNA-containing long primary transcripts ( $< 2,000$  nt) in addition to

transcripts of about 300 nt and 90 nt (Appendix Fig S5D). This finding is consistent with the *alu*RNA length distribution of nucleolar *alu*RNA as inferred from the RNA-seq data (Appendix Fig S4). Thus, we conclude that Pol II-dependent *alu*RNAs are largely over-represented in nucleoli.

### Changes in *alu*RNA levels affect nucleolar structure and rRNA synthesis

Next, we tested whether ectopic *alu*RNA was capable of rescuing  $\alpha$ -amanitin-induced perturbation of nucleolar organization. Indeed, microinjection of *in vitro* transcribed *alu*RNAs triggered reassembly of nucleolar bodies after  $\alpha$ -amanitin inhibition of Pol II (Fig 3B). The forward *alu*RNA variant was more efficient in rescuing nucleolar dispersion than the reverse *alu*RNA or an L1-repeat RNA transcript (Fig 3B and Appendix Table S4).

To further investigate the functional relevance of *alu*RNAs for nucleolar structure and function, we depleted *alu*RNA with different specific antisense oligonucleotides (ASOs) (Ideue *et al*, 2009) corresponding to 20 nucleotides of the nucleolar *alu*RNA consensus sequence (Appendix Fig S3 and Appendix Table S4). The ASOs, which were transfected into the cell via transfection reagent, hybridized to the target RNAs that were subsequently cleaved by endogenous RNase H. Knockdown of *alu*RNA, as measured from RNA-seq analysis (Appendix Fig S6A and B), preserved the level of housekeeping genes (Appendix Fig S6C) (Eisenberg & Levanon, 2013) but produced a phenotype resembling that observed after  $\alpha$ -amanitin treatment: dispersion of nucleoli and the nucleolar marker protein NPM (Fig 4A and Appendix Fig S1D and E), reduction in *alu*RNA FISH signal (Fig 4B and Appendix Fig S6D) and repression of pre-rRNA synthesis (Fig 4C and D and Appendix Fig S1B and C). In addition,  $\alpha$ -amanitin treatment induced a particular strong reduction in intronic *Alu* repeat-containing transcripts (Appendix Fig S6E), which were included in the sequences targeted by the *alu*RNA ASOs. Furthermore, ASO-mediated knockdown of *alu*RNA triggered the dispersion of nucleolar marker proteins such as NCL, NPM and Pol I (Fig 4A and B and Appendix Fig S7A). This phenotype was not observed in cells treated with ASOs targeting the highly abundant L1-repeat or 7SL RNA families (Appendix Table S4 and Appendix Fig S7B and C), for which cells showed a phenotype similar to the control ASO-treated cells. Notably, dispersion of nucleoli upon depletion of *alu*RNA was not restricted to HeLa cells but also observed in human keratinocytes or fibroblasts (Appendix Fig S7B and C). We conclude from these results that a reduction of *alu*RNA levels induced strong perturbations in nucleolar structure and rRNA synthesis.

Time course analysis by immunofluorescence microscopy revealed that dispersion of nucleoli after *alu*RNA knockdown occurred in two steps. First, the size of nucleoli increased within 1–3 h after  $\alpha$ -amanitin treatment or 6–10 h after knockdown of *alu*RNA (Appendix Fig S8A and B). When nucleoli reached a critical size, they dispersed into smaller particles. Swelling of nucleoli and formation of numerous small ectopic NPM-containing particles were also observed in cells treated with LNA antisense “blocker” probes that were designed to hybridize to *alu*RNAs without inducing their degradation (Appendix Fig S8C). A control LNA blocker directed against L1-repeat transcripts did not disturb nucleolar structures (Appendix Fig S8D).

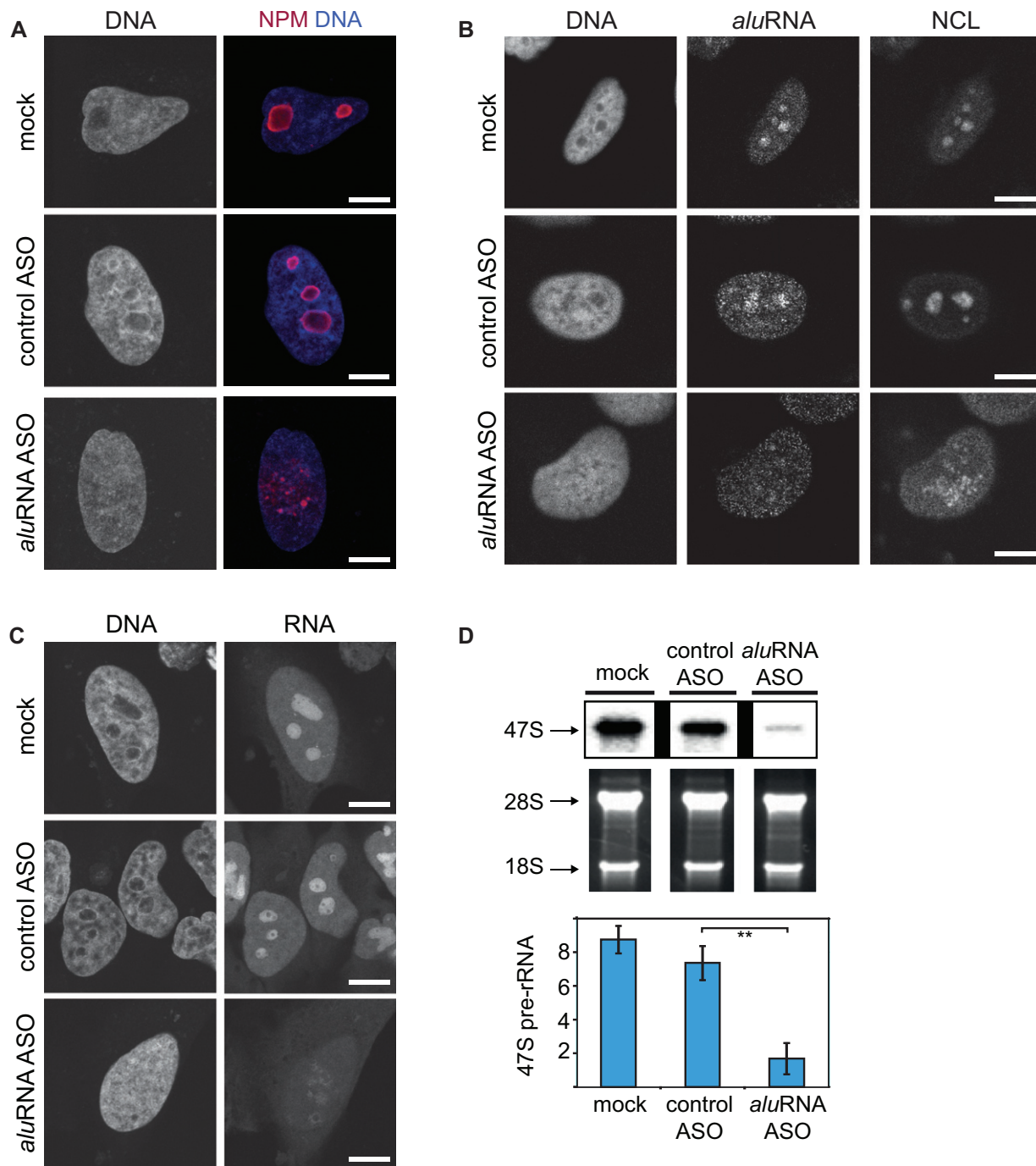


**Figure 4. Knockdown or overexpression of *alu*RNA impact size of nucleoli and rDNA transcription.**

**A** CLSM images showing NPM (immunofluorescence, red) in HeLa cells transfected with control ASO, *alu*RNA ASO, or treated with transfection reagent only (mock). Nuclei were counterstained with DAPI (blue). A fraction of  $80 \pm 8\%$  of the cells treated with *alu*RNA ASO ( $n = 143$ ) showed irregular nucleoli or dispersed nucleoli (53% of the cells). Only  $26 \pm 9\%$  of the cells treated with control ASO presented abnormal nucleoli, with none of them showing a dispersion of nucleolar domains ( $n = 123$ ),  $P$ -value  $< 0.01$ ,  $t$ -test.

**B** CLSM images showing NCL localization (immunofluorescence), *alu*RNA (RNA FISH) and DNA (DAPI). Transfection of HeLa cells was done as in (A).

**C** HeLa cells were transfected as in (A), and nascent RNAs were visualized by pulse labeling with ethynyl uridine (EU) for 30 min. Nuclei were counterstained with DAPI (DNA).

**D** Levels of 47S pre-rRNA in mock-, control ASO- and *alu*RNA ASO-treated HeLa cells. Top: Northern blot. Center: Agarose gel electrophoretic analysis of RNA. Bottom panel: Quantification from RT-qPCR levels of 47S pre-rRNA normalized to 18S rRNA. Error bars represent the standard deviation ( $n = 6$ ). \*\* $P$ -value  $< 0.01$ ,  $t$ -test.

Data information: Scale bars, 10  $\mu$ m. See also Appendix Figs S1C, S6, S7 and S8, Appendix Table S4.

Source data are available online for this figure.

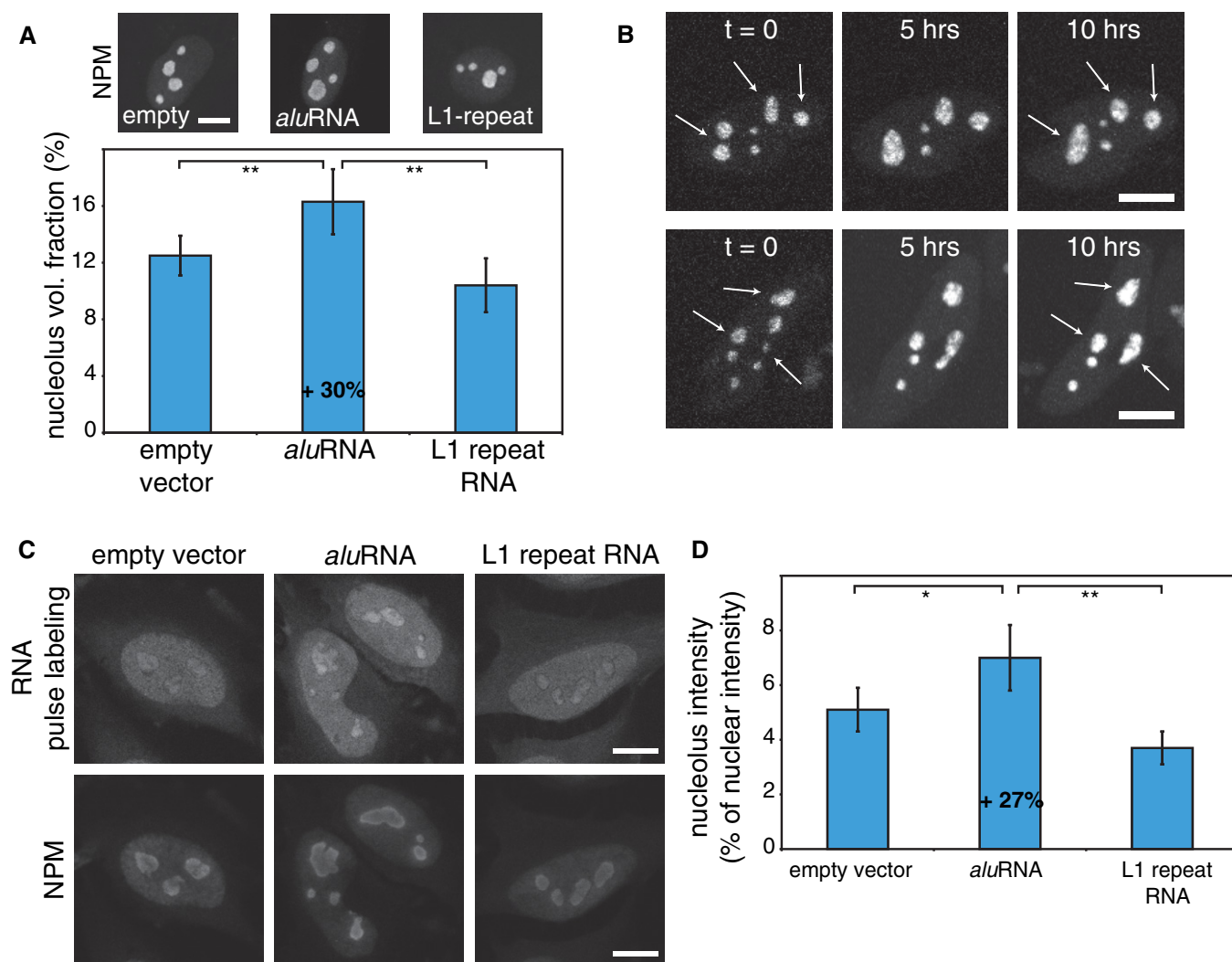


**Figure 5. *alu*RNA overexpression induces an increase in nucleolar volume and activity.**

- A** HeLa cells were transfected with an empty vector or plasmids expressing *alu*RNA or L1-repeat RNA and GFP from a separate promoter. Transfected cells were identified by GFP fluorescence, and nucleoli volumes were evaluated based on the immunofluorescence signal of the nucleolar marker NPM. The graphs show that the volume of nucleoli is increased by 30% in the presence of ectopic *alu*RNA ( $\pm$  95% CI,  $n = 20$ ). \*\* $P$ -value < 0.01,  $t$ -test. Scale bar, 10  $\mu$ m.
- B** CLSM live-cell imaging of RFP-NCL in cells transfected with a plasmid expressing *alu*RNA and imaged for 10 h. The arrows indicate nucleolar domains displaying time-dependent increase in the nucleolar size or fusion of two domains into one. Scale bars, 10  $\mu$ m.
- C** HeLa cells were transfected as in (A) and incubated for 24 h. Nascent RNA was pulse-labeled for 30 min, and nucleoli were visualized by immunofluorescence of NPM. Scale bars, 10  $\mu$ m.
- D** Graphs represent the intensity of nucleolar fluorescence signals as percentage of the intensity of nuclear signals and reveal a 27% increase in the presence of ectopic *alu*RNA ( $\pm$  95% CI,  $n = 30$ ). \*\* $P$ -value < 0.01, \* $P$ -value = 0.01,  $t$ -test.

To examine whether overexpression of *alu*RNA would increase the size of nucleoli, we transfected cells with a plasmid that simultaneously expresses GFP from a Pol II CMV promoter and RNAs from a Pol III U6 promoter. As shown in Fig 5A, the size of nucleoli increased by 30% upon overexpression of forward *alu*RNA, as quantified by 3D measurements of imaging stacks. In contrast, overexpression of an L1-repeat transcript had no significant effect. This finding was confirmed by tracing single living cells over time using an RFP-tagged NCL as nucleolar marker. Clearly, overexpression of the forward *alu*RNA sequence resulted in an enlargement of nucleoli within a single cell over a time period of 10 h (Fig 5B). In addition, RNA pulse labeling of nascent RNA under the same conditions revealed an

increase in nucleolar activity by 27% in the presence of ectopic *alu*RNA, but not of L1-repeat RNA, based on measuring the nucleolar RNA fluorescence signal intensity (Fig 5C and D). Thus, both the loss-of-function and the gain-of-function experiments showed a consistent correlation between *alu*RNA levels, nucleoli size and rRNA production.

#### B1-containing RNAs maintain nucleolar structure in mouse cells

We observed that the structure of nucleoli was also disrupted in mouse NIH 3T3 cells upon Pol II inhibition in a manner very similar to what we found in human cells (Fig 6A) (Caudron-Herger et al,

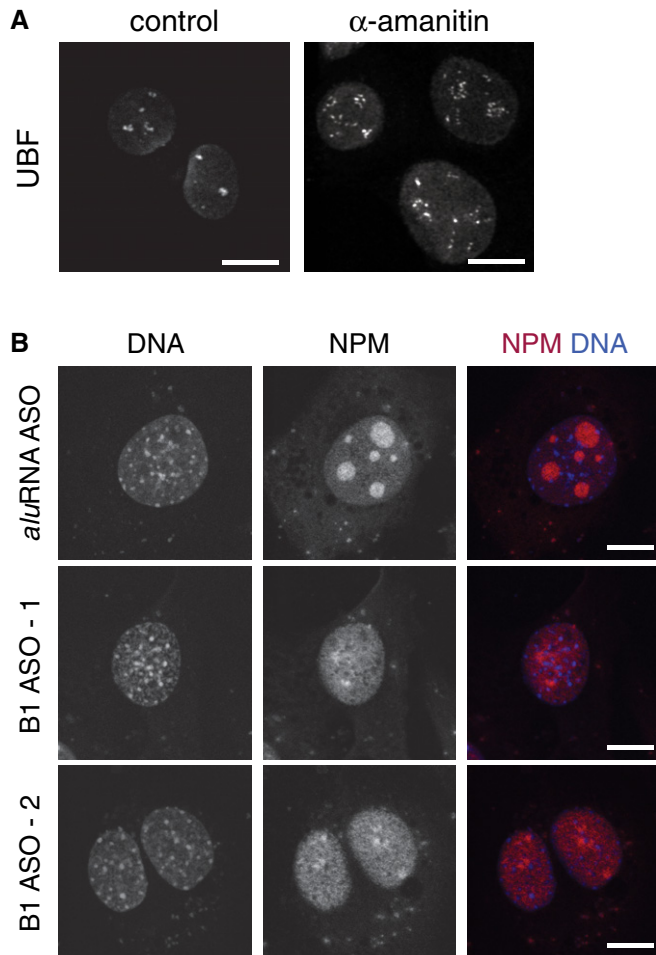


**Figure 6. Nucleoli disruption in mouse cells by depletion of B1-containing RNAs.**

A CLSM images of UBF immunofluorescence in mouse NIH 3T3 cells treated for 5 h with  $\alpha$ -amanitin to inhibit Pol II transcription show the dispersion of nucleoli, as previously also imaged via RNA staining (Caudron-Herger *et al*, 2011).

B CLSM images showing the localization of NPM (immunofluorescence, red) in mouse NIH 3T3 cells treated with ASO as indicated and counterstained with DAPI (blue).

Data information: Scale bars, 10  $\mu$ m.

2011). Accordingly, we investigated whether this phenotype could be assigned to a specific type of RNA transcripts in this organism. *Alu* elements are primate specific (Liu *et al*, 2009), but the closely related B1 repeats are present in the mouse genome (Nishihara *et al*, 2002). We hypothesized that transcripts from B1 elements could represent the functional equivalent of human *alu*RNAs. This assumption was validated by our observation that treatment with ASOs against B1-containing RNA transcripts (Appendix Table S4) induced a significant 30% reduction of B1-containing RNA levels ( $P$ -value = 0.04,  $n$  = 3) and nucleolar dispersion in NIH 3T3 cells (Fig 6B), similar to that revealed in human cell lines (Fig 4A and Appendix Fig S7B and C). As expected, the human *alu*RNA ASO had no effect on nucleolar structure in the mouse fibroblast cell line demonstrating specificity. Thus, B1-containing RNA transcripts are important to maintain nucleolar structure in mouse cells.

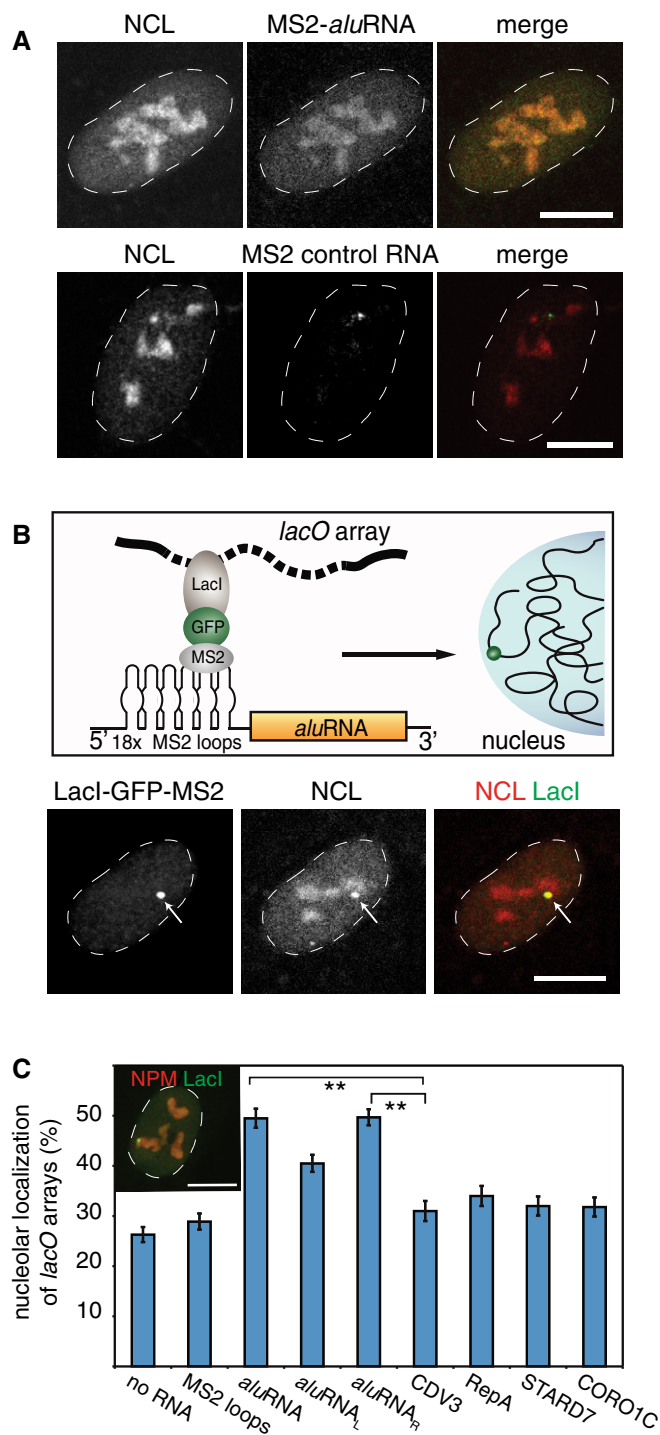
### *alu*RNA interacts with NCL and targets genomic loci to the nucleolus

To further investigate the link between *alu*RNA and nucleolar organization, we conducted a set of experiments with forward *alu*RNA fused to MS2 stem-loop hairpins (MS2-*alu*RNA). First, we observed that ectopically expressed MS2-*alu*RNA was enriched in nucleoli (Fig 7A) as compared to a control RNA sequence. This supports our previous conclusion of *alu*RNA being enriched in the nucleolus that was based on the analysis of endogenous *alu*RNAs by deep sequencing (Fig 2C) and by RNA FISH (Fig 3A). Next, we made use of a U2OS cell line (F4IIB8) containing a stably integrated *lacO* array at a single genomic locus (Jegou *et al*, 2009). We used a *lac* repressor (LacI) protein construct fused to the MS2 stem-loops binding protein (Shevtsov & Dundr, 2011) to recruit MS2-RNAs to the *lacO* array (Fig 7B). Notably, we observed that MS2-*alu*RNA<sub>R</sub> induced recruitment of NCL to the *lacO* array (Fig 7B). Furthermore, tethering of both MS2-*alu*RNA and MS2-*alu*RNA<sub>R</sub> variants to these sites significantly increased the number of *lacO* arrays localizing in nucleoli (Fig 7C). These observations suggest that *alu*RNA interacts with NCL and can target genomic loci to nucleoli.

### Nucleolin and nucleophosmin interact with *alu*RNA and target genomic loci to the nucleolus

To elucidate the mechanism by which *alu*RNA targets genomic loci to the nucleolus, we investigated the interaction of *alu*RNAs with specific nucleolar proteins. We analyzed the association of *alu*RNA with NCL and NPM, abundant nucleolar proteins that interact with RNA and are important for the structure of nucleoli (Ugrinova *et al*, 2007; Amin *et al*, 2008) using a U2OS cell line (F6B2) that contains three *lacO* array integrations at different chromosomes (Jegou *et al*, 2009). To visualize recruitment of GFP-tagged proteins to the *lacO* arrays, a previously described fusion construct of LacI with a GFP-binding protein was used (Chung *et al*, 2011) (Fig 8A). Analysis of the localization of *alu*RNA by RNA FISH revealed that *alu*RNA was enriched at *lacO* arrays that were associated with GFP-tagged NCL or NPM (Fig 8A and Appendix Fig S9A). Interestingly, GFP-tagged fibrillarin, involved in the site-specific 2'-O-methylation of ribose (Reichow *et al*, 2007), was also recruiting *alu*RNA at the *lacO* arrays (Appendix Fig S9A). In contrast, only background levels of *alu*RNA were found at *lacO* arrays associated with GFP or the RNA-binding domain of TIP5, a subunit of the nucleolar remodeling complex NoRC (Fig 8A) (Mayer *et al*, 2006). Moreover, recruitment of NCL to *lacO* arrays was accompanied by enrichment of UBF and NPM (Appendix Fig S9B), confirming previously reported interactions between NCL, UBF and NPM (Li *et al*, 1996; Hisaoka *et al*, 2010).

Next, we evaluated the localization of the *lacO* arrays upon tethering of tagged NCL, NPM or fibrillarin. We found that NCL or NPM targeted 60–70% of the megabase-long *lacO* arrays to nucleoli (Fig 8B and Appendix Fig S9C). In contrast, GFP or GFP-tagged fibrillarin failed to promote the translocation of the *lacO* arrays to nucleoli (Fig 8B and Appendix Fig S9C). Moreover, deletion of the RNA-binding domains and the C-terminal GAR domain of nucleolin (NCL- $\Delta$ RNA) abolished its nucleolar enrichment, interaction with NPM and, importantly, nucleolar targeting of the *lacO* arrays (Fig 8B and Appendix Fig S9D).



The interaction of NCL with *aluRNA* variants was further confirmed by pull-down assays using nuclear extracts and biotinylated *aluRNA* transcripts immobilized to streptavidin beads (Appendix Fig S9E). Even when raising the salt concentration up to 450 mM, a stable NCL-*aluRNA* interaction was found in the pull-down (Appendix Fig S9F). However, under the same experimental conditions and even at lower salt concentrations, no interaction between NPM and *aluRNA* was observed (Appendix Fig S9G).

**Figure 7. Ectopically expressed *aluRNA* accumulates in the nucleolus together with associated genomic loci.**

**A** CLSM images of MS2-tagged *aluRNA* or MS2-tagged control RNA (a fragment from the transcript of the CDV3 gene). MS2-loop-containing RNAs were visualized by RNA FISH using MS2-loop-specific FISH probes (green); nucleoli were visualized by immunofluorescence of NCL (red).

**B** The top panel depicts the experimental approach used to tether MS2-loop-containing RNAs to *lacO* arrays via a GFP-tagged LacI-MS2 coat fusion protein. The *lacO* arrays were stably integrated in the genome of U2OS cells. In the bottom panel, CLSM images of U2OS cells are shown that were transfected with MS2-*aluRNA<sub>R</sub>*. They reveal the localization of LacI-GFP-MS2 and NCL (immunofluorescence, red). The arrow indicates the *lacO* array, which is associated with a nucleolar domain.

**C** MS2-loop-containing forward *aluRNA* or *aluRNA<sub>L</sub>* or *aluRNA<sub>R</sub>* were recruited to the single stably integrated *lacO* array in the U2OS F41B8 cell line. The propensity for nucleolar localization was evaluated as the average number of *lacO* arrays with tethered RNA detected in nucleoli ( $\pm$  95% CI) and is plotted in the bar chart. Calculations are based on analysis of more than 100 cells. \*\**P*-value < 0.01, *t*-test, from the analysis of two independent biological replicates. As controls, transcripts of the MS2 loops only, the MS2-CDV3, MS2-RepA, MS2-STARD7 and MS2-CORO1C RNAs were used. The inset shows a CLSM image with MS2-GFP-LacI (green) and NPM (red, immunofluorescence) after recruitment of MS2-*aluRNA*.

Data information: Scale bars, 10  $\mu$ m.

In support of our conclusion that *aluRNA* interacts with NCL and may indirectly involve NPM to maintain the structure of nucleoli, simultaneous siRNA-mediated knockdown of NCL and NPM yielded a phenotype very similar to that observed after  $\alpha$ -amanitin treatment or *aluRNA* knockdown. Notably, dispersion of nucleoli and redistribution of rDNA throughout the nucleoplasm were more pronounced in cells depleted of both, NPM and NCL, compared to cells depleted of one of the two proteins only (Fig 8C and Appendix Fig S9H and I). Together, these results demonstrate that tethering of NCL, NPM and *aluRNA* to chromatin is sufficient to target large genomic regions to the nucleolus and strongly suggest that the interaction of NCL with *aluRNA*, and co-recruitment of NPM, is important to build up a functional nucleolus.

## Discussion

In previous studies, it has been shown that number, size and morphology of nucleoli are closely related to rRNA production and the activity of chromatin modifiers (Laferte *et al*, 2006; Boisvert *et al*, 2007; Hernandez-Verdun *et al*, 2010; Pontvianne *et al*, 2013). Through its dynamic structural properties, the nucleolus can act as a cellular stress sensor (Rubbi & Milner, 2003; Olson, 2004; Sirri *et al*, 2008; Boulon *et al*, 2010). Here, we were able to link a fraction of intronic *Alu* element-containing Pol II transcripts termed *aluRNA* with an essential role for maintaining nucleolar structure and function. These RNAs are part of the large fraction of about 50% of the total pool of genomic *Alu* repeats that reside in introns (Deininger, 2011). Loss of *aluRNAs* due to Pol II inhibition or ASO knockdown led to dispersion of nucleoli into smaller domains and reduction in rDNA transcription (Figs 1A and 4 and Appendix Fig S1B and C). In contrast, microinjection of *in vitro* transcribed *aluRNA* promoted nucleolar (re)assembly (Fig 3B). These activities were most pronounced for the forward *aluRNA*-type sequence, which was highly enriched in

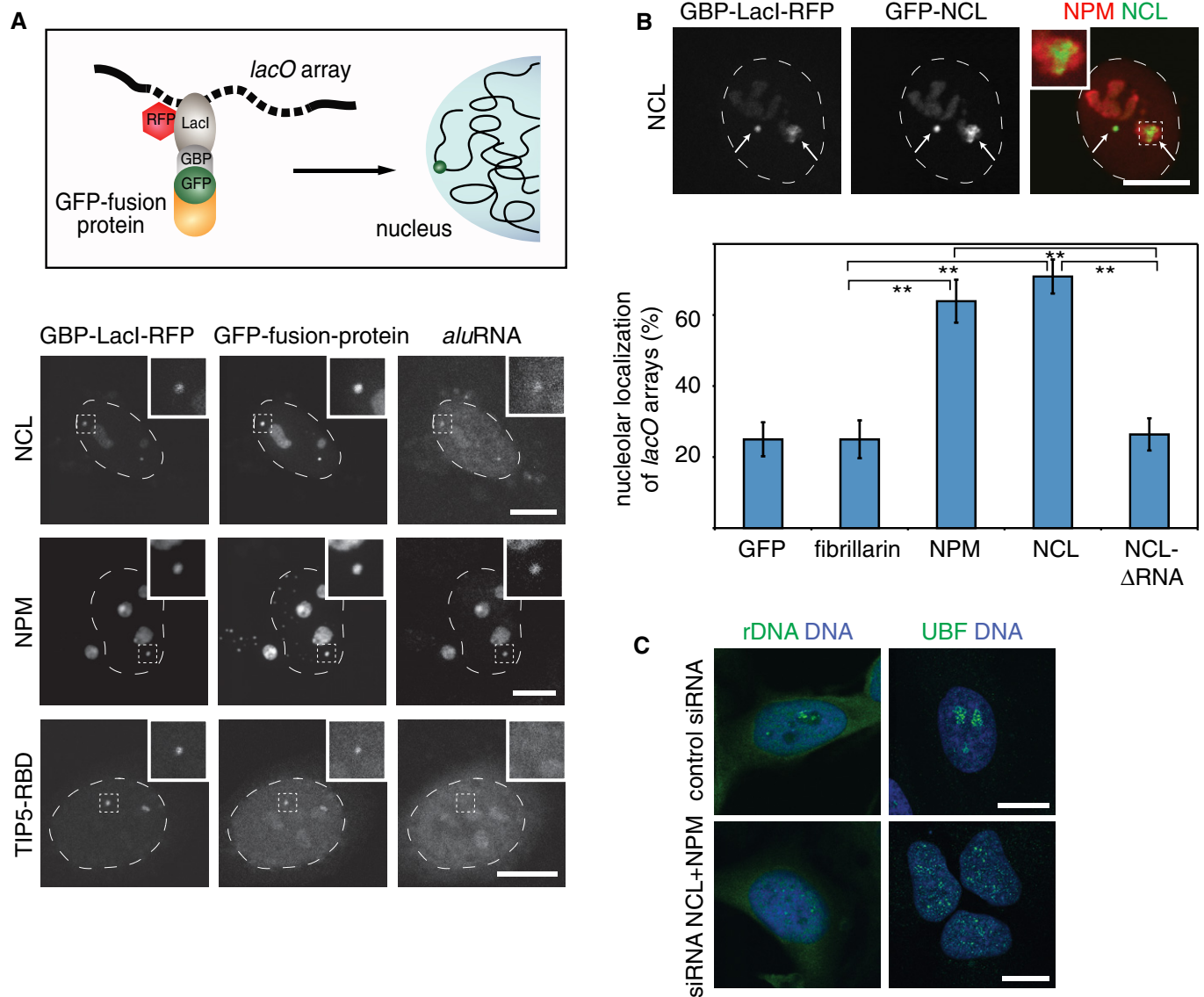


**Figure 8. NCL and NPM interact with *alu*RNA and target genomic loci to the nucleolus.**

**A** Top: Scheme illustrating the experimental approach used to tether GFP-tagged LacI fusion proteins via a GFP-binding protein (GBP) to *lacO* arrays. The *lacO* arrays are stably integrated in the genome of U2OS cells. Bottom: CLSM images showing the localization of GBP-LacI-RFP, GFP-NCL, GFP-NPM or GFP-TIP5-RBD fusion proteins relative to *alu*RNA that was visualized by RNA FISH. The insets contain an enlarged image of one of the *lacO* loci.

**B** CLSM images showing GBP-LacI-RFP and GFP-NCL (green) recruited to *lacO* arrays as indicated by arrows. Immunofluorescence of endogenous NPM (red) marks nucleoli. The inset shows decondensation of *lacO* arrays in the nucleolus. The graph at the bottom depicts the average number of *lacO* loci tethered to nucleoli ( $\pm$  95% CI) by the indicated proteins ( $n = 72$ ). NCL-ΔRNA is an NCL deletion mutant lacking the RBD and GAR domains required for RNA binding. \*\* $P$ -value < 0.01,  $t$ -test.

**C** CLSM images of UBF (immunofluorescence, green) or rDNA (DNA FISH, green) and DNA (DAPI, blue) after knockdown of NCL and NPM by siRNA in HeLa cells.

Data information: Scale bars, 10  $\mu$ m.

See also Appendix Fig S9.

the nucleolus as shown by RNA-seq (Fig 2) and RNA FISH (Fig 3A). Based on the RNA-seq (Appendix Fig S4) and Northern blot analysis (Appendix Fig S5D), we conclude that relatively short *Alu* element-containing RNAs of 100–300 nt in size are stably present in the cell. This finding is consistent with a previous study that identified a class of intron-encoded Pol II *Alu*-related transcripts of 100–200 nt in length termed AluACA RNAs in the nucleus (Jady *et al*, 2012). We found no evidence

that the expression of *alu*RNAs was also related to Pol III transcription although *Alu* elements contain an internal Pol III promoter in their left arm (Dieci *et al*, 2007). Consistently, Pol III inhibition was neither associated with nucleolus dispersion nor with the reduction in pre-rRNA synthesis (Fig 1A and Appendix Fig S1B and C). It is noted that the internal Pol III promoter, which differs from the original sequence found in the 7SL RNA, is relatively weak and subject to additional silencing

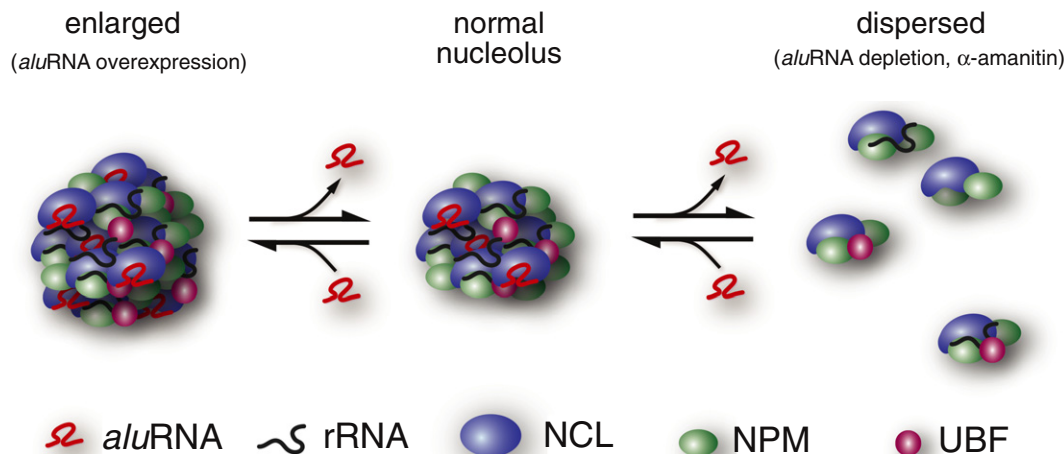


**Figure 9. Model of *alu*RNA-driven maintenance of the nucleolus.**

The knockdown of *alu*RNA or treatment with  $\alpha$ -amanitin induces the segregation of nucleolar compartments into smaller domains (dispersion process) as observed (Figs 1A and 4A, and Appendix Fig S2). With regard to rRNA production, those "droplets," which may vary in composition, are less efficient but some rRNAs are still produced albeit at low levels (Appendix Fig S1B and C and Fig 4C and D). Overexpression of *alu*RNA promotes assembly into larger nucleolar subcompartments, with enhanced Pol I activity (see Fig 5). This model is in excellent agreement with the previously reported liquid-like model of the nucleolus (Brangwynne *et al.*, 2011; Weber & Brangwynne, 2012) and suggests a RNA binding-driven liquid-like transition between dispersed nucleolar domains and intact and fully functional nucleoli.

mechanisms (Li & Schmid, 2001; Hasler & Strub, 2006). Accordingly, *Alu* repeat expression in general is dependent on promoters located in their flanking regions (Roy *et al.*, 2000). We conclude that maintenance of nucleolar structure is related to Pol II activity by spliced out *alu*RNAs from Pol II transcripts. In turn, this affects rRNA synthesis since Pol I transcriptional activity is intrinsically linked to nucleolar structure and suggests that the amount of Pol II-produced *alu*RNA modulates Pol I transcription levels.

In agreement with a role of *alu*RNA in promoting nucleolar domain assembly, we observed that overexpression of *alu*RNA induced an increase in nucleolus size as well as an enhanced nucleolar transcriptional activity (Fig 5). Accumulation of *Alu* repeat-containing RNA transcripts beyond a critical level can also become cytotoxic for the cell as reported previously for retinal pigmented epithelium (Kaneko *et al.*, 2011). This phenotype was linked to a deficit in DICER, a component of the RNA-induced silencing complex (Kaneko *et al.*, 2011). Interestingly, a significant increase in nucleolar size was observed in cells depleted of DICER (Liang & Crooke, 2011). These previous studies suggest that *Alu* repeat-containing RNA levels are also subject to post-transcriptional regulation. Furthermore, they corroborate our own observation that overexpression of *alu*RNA induces the formation of larger nucleoli.

Our analysis suggests that *alu*RNA exerts its nucleolar maintenance activity via interaction with nucleolar proteins. Using the *lacO* array recruiting system (Figs 7 and 8), we detected binding of *alu*RNA to NCL and NPM in living cells. Our additional pull-down experiments confirmed an efficient interaction of NCL with *alu*RNA but also with other RNAs (Appendix Fig S9E) in addition to the previously reported NCL–rRNA interaction (Tajirishi *et al.*, 2011). It is noted that the concentration of a given NCL–RNA complex will be proportional to the product of the association

constant and respective RNA binding site concentration. Given that *alu*RNAs are highly abundant, this would favor their NCL binding over that of other RNA species to some extent. Nevertheless, it appears likely that the ~100-fold enrichment of *alu*RNA in the nucleoplasm cannot be explained solely by binding to soluble NCL in the nucleoplasm but involves additional interactions with other nucleolar proteins, RNAs or DNA components within the nucleolus. Furthermore, our data suggest that a possibly indirect NPM–*alu*RNA recruitment occurs in the cell as detected in the *lacO* experiments. It might contribute to the *alu*RNA enrichment directly in the nucleolus, where NPM can additionally interact with UBF and rRNA (Hisaoaka *et al.*, 2010).

In support of *alu*RNA promoting nucleolar assembly, recruitment of *alu*RNA and/or NCL and NPM to *lacO* arrays led to a significantly increased nucleolar localization of these arrays. This raises the question how intron-encoded nucleolar *alu*RNA exerts such an activity. A possible mechanism is related to the physico-chemical properties of RNA–protein interactions (Weber & Brangwynne, 2012). According to the liquid-drop model of the nucleolus proposed previously, unmixing of nucleolar components from the surrounding nucleoplasm as observed here for NCL/NPM and *alu*RNA is due to their interaction properties (Brangwynne *et al.*, 2011). Notably, both NCL and NPM contain disordered and low-complexity sequences (Emmott & Hiscox, 2009; Hisaoaka *et al.*, 2014). These sequences form protein domains that are able to drive RNA-dependent intracellular phase-separation processes in the cell through conformational changes upon RNA binding (Han *et al.*, 2012; Hyman & Simons, 2012; Weber & Brangwynne, 2012). Such a behavior has been reported for NPM (Hisaoaka *et al.*, 2010, 2014). It is consistent with our findings of an emulsion-like dispersion of the nucleolus observed after Pol II inhibition or *alu*RNA depletion (Appendix Fig S8A and B) as well as a RNA-dependent nucleolar targeting

activity of NCL (Fig 8B). In such a scenario, *alu*RNA would serve as “glue” or scaffold to orchestrate nucleolus formation via promoting the self-organization of NCL/NPM-containing “droplets” into domains that efficiently associate with rDNA and support Pol I transcriptional activity within the nucleolus (Fig 9). This could serve to increase the local concentration of reactants and the efficiency of rRNA synthesis (Boisvert *et al*, 2007; Weber & Brangwynne, 2012).

NCL, NPM and fibrillarin are constituents of the prenucleolar bodies that associate with the nucleolar organizer regions at early G<sub>1</sub> phase (Dousset *et al*, 2000). Their enrichment at rDNA loci could originate from a direct interaction of NCL with rDNA (Olson *et al*, 1983). At the same time, UBF has been identified as a key player in nucleating the assembly of nucleoli (Grob *et al*, 2014). It suggests that the *alu*RNA-directed fusion into larger domains could occur via the interaction of NCL and/or NPM with UBF bound to nucleolar organizer regions. Consistent with this view and in accord with the observation that NCL co-localizes with UBF and interacts with NPM (Li *et al*, 1996), we show that recruitment of NCL to *lacO* arrays was accompanied by the enrichment of both UBF and NPM at these arrays (Appendix Fig S8B). Thus, the assembly of the nucleolus requires multiple coordinated macromolecular interactions including: (i) DNA–protein interactions such as binding of UBF to rDNA and possibly direct interactions of NCL with rDNA (Olson *et al*, 1983; Cong *et al*, 2012); (ii) protein–protein interactions as, for example, interaction of NCL with UBF and NPM, or NPM with UBF (Hisaoka *et al*, 2010); and (iii) RNA–protein interactions that involve the association of *alu*RNA with NCL and other nucleolar components as suggested here.

The nucleolus is a nuclear subcompartment that is found in almost all eukaryotic cells (Lamaye *et al*, 2011), while *Alu* elements are primate specific (Liu *et al*, 2009). This raises the question whether the mechanism revealed here in studying human cells can also operate in other eukaryotic organisms. In favor of this possibility, we found that nucleoli in mouse fibroblast cells showed a similar disruption of their structure upon Pol II inhibition (Fig 6A) and observed that ASO targeting of *Alu*-related B1 repeat-containing RNAs induced nucleolar disassembly (Fig 6B). This strongly suggests that transcripts from B1 elements could represent the functional equivalent of human *alu*RNAs. It is noted that *Alu* and B1 repeats have a common ancestor in evolution, namely the 7SL RNA (Nishihara *et al*, 2002). This RNA is a crucial component of the signal recognition particle and is present in all eukaryotic cells (Nagai *et al*, 2003). One could speculate that RNAs derived from the 7SL RNA family share a common function for nucleolus structure throughout eukaryotic organisms.

Maintaining large numbers of *Alu* repeats in the human genome imposes a significant risk to genome stability (Callinan & Batzer, 2006; Belancio *et al*, 2010). Furthermore, intronic *Alu* elements may also compromise correct mRNA production. As reported recently, the cell has developed a dedicated mechanism to prevent misguided splicing that would lead to exonization of intronic *Alu* repeats (Zarnack *et al*, 2013). The important function of *alu*RNA to maintain a functional nucleoli structure revealed in our study could represent a selection pressure to keep *Alu* sequences in introns.

## Materials and Methods

### Cell culture and purification of nucleoli

HeLa and HeLa S3 cells were grown at 37°C/5% CO<sub>2</sub> in RPMI 1640 or DMEM containing 1 g/l glucose, respectively, and supplemented with 10% FCS, 2 mM L-glutamine and 1% penicillin/streptomycin. U2OS and NIH 3T3 cells were cultured under the same conditions in DMEM containing 1 g/l or 4.5 g/l glucose, respectively. The U2OS cell clones F6B2 (stable insertion of three *lacO* arrays) and F4IIB8 (stable insertion of one *lacO* array) and transfection of cells with expression plasmids for *lacO* array tagging and protein recruitment were conducted as described previously (Jegou *et al*, 2009; Chung *et al*, 2011). The human keratinocyte and fibroblast cells were kindly provided by Aubry Miller and Nikolas Gunkel (German Cancer Research Center, Germany).

Nucleoli were isolated from HeLa S3 cells as described (Busch *et al*, 1963; Sullivan *et al*, 2001), and RNA was purified from unfractionated cells (total RNA) or nucleoli by TRIzol (Caudron-Herger *et al*, 2011). Pre-rRNA and *alu*RNAs from total RNA were assayed by Northern blotting using a radiolabeled 5'-ETS antisense riboprobe (from +150 to +1) or a radiolabeled antisense *Alu* probe (Appendix Table S4). Alternatively, pre-rRNA levels were quantified by RT-qPCR as reported before (Hoppe *et al*, 2009). Quantification of rRNA amounts depends on synthesis and degradation rates. 47S has a very short half-life time in the range of minutes (Popov *et al*, 2013) as compared to 18S and 28S that are stable for days (Defoiche *et al*, 2009). Therefore, 47S steady-state measurements can be correlated with the synthesis rate of the precursor (before the cleavage of the 5'-ETS), as done here.

### Drug treatments

RNA polymerases were inhibited by culturing cells for 5 h in medium supplemented with the following inhibitors: actinomycin D (AMD, 50 ng/ml) for Pol I,  $\alpha$ -amanitin (50  $\mu$ g/ml) or 5,6-dichloro-1-beta-D-ribofuranosylbenzimidazole (DRB, 50  $\mu$ g/ml) for Pol II, and ML-60218 (2-chloro-N-[3-(5-chloro-3-methylbenzo[b]thien-2-yl)-1-methyl-1H-pyrazol-5-yl]-benzenesulfonamide) for Pol III. Translation was inhibited by cycloheximide treatment (50  $\mu$ g/ml) for 5 h.

### Microinjection

Microinjection of cells grown in Nunc Lab-Tek chamber slides in F-15 medium (Thermo Scientific) was performed with a computer-assisted system (AIS2, CellBiology Trading). A volume of about 50 femtoliters was injected using a needle with a tip diameter of about 300 nm, 150 hPa pressure and 0.5 s injection time. Ten microliters of injection mix contained 2  $\mu$ l propidium iodide (PI, 1 mg/ml, Thermo Fisher Scientific) and 1  $\mu$ g of RNA in PBS. Following injection, cells were cultured under standard conditions for 30 min and processed for confocal microscopy image acquisition.

### Immunofluorescence and RNA labeling

Cells grown on coverslips were fixed 24 h after transfection with 4% paraformaldehyde/PBS. For immunostaining, cells were

permeabilized for 5 min with ice-cold 0.5% (v/v) Triton X-100/PBS. After three washes, samples were incubated for at least 15 min with 10% goat serum in PBS followed by addition of antibodies specific to NCL (sc-13057), NPM (sc-56622), UBF (sc-13125), SC35 (BD Pharmingen, 556363) or Pol I (Percipalle *et al*, 2006) for 1 h at room temperature (NCL, Pol I) or overnight at 4°C (NPM, UBF). After washing, cells were incubated for 25 min with the appropriate secondary antibodies conjugated to Alexa Fluor 488, 568 or 633 (Thermo Fisher Scientific, Molecular Probes) and for another 5 min with 4',6-diamidino-2-phenylindole dihydrochloride (DAPI). The coverslips were mounted with Mowiol. For pulse labeling of RNA, cells were incubated for 30 min with 1 mM 5-ethynyl uridine (EU) and fixed with 4% paraformaldehyde/PBS. EU-labeled transcripts were detected using Alexa Fluor 488 azide (Click-it RNA imaging Kit, Thermo Fisher Scientific).

### DNA and RNA FISH

For DNA FISH, cells grown on coverslips were fixed with 4% paraformaldehyde/PBS, washed in PBS and permeabilized with 0.5% (v/v) Triton X-100/PBS. After serial washes with ethanol (70, 80 and 100%) and air-drying, DNA was denatured at 80°C for 5 min and hybridized overnight at 42°C to a biotin-labeled human rDNA probe (from nucleotides 18063 to 30486, GenBank Accession No.: U13369.1) in hybridization buffer (50% formamide, 2× SSC and 10% dextran sulfate). The plasmid pHr4 (Mais *et al*, 2005), a kind gift from Brian McStay (NUI Galway, Ireland), was used to generate about 2,500-bp-long body-labeled fragments by nick translation. Slides were washed consecutively with hybridization buffer, 2× SSC, 0.2× SSC containing 0.1% (v/v) Tween-20 at 55°C, 2× SSC containing 0.05% (v/v) Tween-20 and finally PBS.

For RNA FISH, cells grown on coverslips were permeabilized in CSK buffer (100 mM NaCl, 300 mM sucrose, 3 mM MgCl<sub>2</sub>, 10 mM PIPES, 0.5% (v/v) Triton X-100) containing 10 mM vanadyl ribonucleoside complex (VRC) or 50 µg/ml RNase A. Cells were fixed with 4% paraformaldehyde/PBS, dehydrated by sequential washes with ethanol (70, 85 and 100%) and air-dried. The RNA was hybridized overnight in hybridization buffer at 37°C with 2.5 µl of digoxigenin-labeled *alu*RNA or control RNA probes (each 50 ng/µl). Slides were washed consecutively with hybridization buffer, 0.2× SSC containing 0.1% (v/v) Tween-20 at 40°C, 2× SSC, and PBS. Digoxigenin-labeled RNA was detected with anti-digoxigenin antibody (Roche, clone 1.71.256). The MS2 RNA stem-loops were visualized using a 5'-Atto-565-labeled antisense probe that targets the MS2 loop sequence (Chaumeil *et al*, 2002). Sequences of the FISH probes are listed in Appendix Table S4.

### Plasmids and *in vitro* transcription

GFP-tagged proteins were generated by cloning the corresponding cDNAs into pEGFP-C1 (Thermo Fisher Scientific). The pEGFP-NCL and pEGFP-fibrillarin vectors were obtained from Addgene (#28176 and #26673, respectively). pTagRFP-NCL was produced by cloning the NCL into KpnI and BamHI sites of the pTagRFP plasmid (Evrogen). pEGFP-NPM was kindly provided by Mitsuru Okuwaki (University of Tsukuba, Japan). GFP-TIP5-RBD and GBP-LacI-mRFP plasmids have been described (Jegou *et al*, 2009; Zillner *et al*,

2013). The GFP-NCL-ΔRNA deletion mutant missing the RBD and GAR domains was generated by cloning of the corresponding cDNA PCR fragment into the KpnI and BamHI sites of the pEGFP-C1 plasmid. MS2 coat protein fused to GFP-LacI was cloned by introducing the MS2 protein into the NheI and AgeI sites of pSV2-GFP-LacI (Jegou *et al*, 2009). The MS2-*alu*RNA and the corresponding control RNA sequences were synthesized as DNA (Integrated DNA Technologies, Inc) and were cloned into a pcDNA3 plasmid containing 18 repeats of the MS2 stem-loop as described (Schmidt *et al*, 2011). The MS2-*alu*RNA was cloned using the AgeI and NotI restriction sites, and the control sequences were cloned into the NotI site. The sequences are listed in Appendix Table S4. The *alu*RNA and L1-repeat sequences were introduced into the pBS/U6 plasmid expressing either GFP or TagRFP using two BbsI restriction sites (Grimm *et al*, 2006). The plasmid was kindly provided by Dirk Grimm (University of Heidelberg, Germany).

DNA templates for *in vitro* transcription of *alu*RNA and L1-repeat (Appendix Table S4) were amplified using genomic DNA from HeLa cells and primers specific to T7 promoter sequences. *In vitro* transcription was performed using the RNA polymerase T7 High Yield RNA Synthesis Kit (NEB) according to the manufacturer's instructions.

### Confocal fluorescence microscopy and image analysis

Imaging was done with a Leica TCS SP5 confocal laser scanning microscope (CLSM) equipped with a HCX PL APO lambda blue 63×/1.4 NA oil immersion objective (Leica Microsystems CMS GmbH, Mannheim, Germany). A near UV diode, diode-pumped solid-state, argon and helium–neon lasers were used for DAPI (λ = 405 nm), Alexa 488 or GFP (λ = 488 nm), Alexa 568 or Atto-565 or TagRFP (λ = 561 nm) and Alexa 633 (λ = 633 nm) excitation. For multi-color analysis, sequential image acquisition was applied and emission detection ranges were adjusted to minimize crosstalk between the different signals. The detection pinhole had a diameter corresponding to one airy disk.

After microinjection, random pictures of microinjected cells were taken and analyzed using ImageJ (Schneider *et al*, 2012). The images were segmented via thresholding, and the function “Analyze Particles” was used to automatically count the number and size of particles in each picture. For nucleoli volume estimation, confocal z-stacks were acquired, each slice was segmented via thresholding, and the function “Analyze Particles” was used to automatically calculate the nucleolar area in each image. Summing and multiplying each area by the z-step provided an estimation of the nucleolar volume. A similar procedure was repeated to evaluate the nuclear volume based on the DAPI staining of the DNA. For live-cells image acquisitions of cells transfected with pBS\_U6\_*alu*RNA and RFP-NCL using X-tremeGENE (Roche Life Science), z-stacks of cells were acquired every 30 min. The microscope was equipped with an incubation chamber allowing normal growth conditions (5% CO<sub>2</sub> and 37°C). To determine the fluorescence intensity of nuclei and nucleoli, each slice was segmented via thresholding and the function “Analyze Particles” was used to automatically calculate the intensities. To determine the position of the *lacO* arrays, the fluorescence signal of GBP-LacI-RFP and a nucleolar marker (labeled with Alexa 633, Thermo Fisher Scientific) were overlaid. *P*-values were calculated according to Student's *t*-test.

## RNA and protein knockdown

For RNA knockdown, cells were transfected with Lipofectamine 2000 according to the manufacturer's instruction (Thermo Fisher Scientific) using 40 nM of antisense oligonucleotides (ASOs), that is *alu*RNA ASO or control ASO (see Appendix Table S4 for sequences) 5'-labeled with Cy3. Unless otherwise indicated (see Appendix Fig S8), cells were fixed 14 h after transfection for 10 min in 4% paraformaldehyde/PBS and processed for immunofluorescence. Custom LNA blocker probes (Exiqon) were designed to functionally inactivate target RNAs. The sequences are listed in Appendix Table S4. For siRNA-mediated knockdown of NCL and NPM,  $1.5 \times 10^5$  cells were transfected with Lipofectamine 2000 and siRNAs against NCL (Dharmacon L-003854-00-0005) or NPM (Dharmacon L-015737-00-0005). ON-TARGETplus Non-targeting Pool (Dharmacon, D-001810-10-50) was used as control siRNA. Forty-eight hours after transfection, cells were processed for immunofluorescence microscopy and rDNA FISH or for Western blot analysis using antibodies against NCL (sc-13057), NPM (sc53175) and histone H3 (ab1791, Abcam).

## Protein pull-down with biotinylated RNA transcript

Cell nuclei were isolated from HeLa S3 to prepare a nuclear extract using nuclear lysis buffer (200 mM NaCl; 20 mM Tris-HCl, pH 8.0; 0.2% Tween-20; 1 mM EDTA; 1 mM EGTA). Biotinylated RNA transcripts were *in vitro* transcribed in the presence of biotin-16-UTP (Sigma-Aldrich). Five micrograms of labeled RNA were incubated with 50  $\mu$ l of streptavidin-coated magnetic beads (Thermo Fisher Scientific) for 30 min at room temperature in 100 mM NaCl solution. Beads were washed in washing buffer (5 mM Tris-HCl, pH 7.5; 0.5 mM EDTA; 0.5 M NaCl; 0.05% Tween-20) and further incubated for 3 h in 70  $\mu$ g or 35  $\mu$ g nuclear extract in a final volume of 100  $\mu$ l. After 3 steps of washing in nuclear lysis buffer, the beads were resuspended in 50  $\mu$ l of nuclear lysis buffer and bound proteins were eluted by adding 3  $\mu$ l of RNase A (10 mg/ml; Thermo Fisher Scientific) for 30 min at 4°C. Beads were retrieved on a magnet, and eluted proteins were analyzed by Western blotting.

## RNA sequencing

Total RNA, nucleoplasmic RNA or nucleolar RNA were isolated from HeLa cells or purified nucleoli, respectively, using the RNeasy Mini Kit (Qiagen). High-throughput RNA sequencing was done with two biological replicates. Ribosomal RNA was removed using the Ribo-Zero rRNA Removal Kit (Epicentre/Illumina) according to the manufacturer's protocol. For the first data set, RNAs were fragmented with the RNA fragmentation reagent kit from Ambion (Thermo Fisher Scientific, AM8740). For Illumina sequencing, libraries were generated according to the standard protocol for mRNA (Illumina) comprising first- and second-strand cDNA synthesis, end repair, addition of a single A base and adapter ligation. PCR products of about 200 bp were excised from a 2% E-Gel Size Select (Thermo Fisher Scientific). After determining the concentration and quality on a Qubit fluorometer (Thermo Fisher Scientific) and Bioanalyzer system (Agilent Technologies), 36-nt-long sequencing reactions were performed on the Illumina GAIIx

platform (Deep Sequencing Core Facility of the Cell Networks cluster of excellence, University of Heidelberg, Germany). For the second data set, strand-specific libraries were prepared using the NEBNext Ultra Directional RNA Library Prep Kit for Illumina (#E7420L, New England BioLabs Inc.). Sequencing of 100-base-pair reads was performed on the Illumina HiSeq 2000 platform (Genomics and Proteomics Core Facility of the DKFZ, Heidelberg, Germany).

## RNA-seq data analysis

RNA-seq reactions were performed with 36-nt and 100-nt read length and yielded the number of total and mapped reads given in Appendix Table S5. Reads were quality-controlled and aligned with Bowtie (Langmead *et al*, 2009) on the GRCh37/hg19 (2009) assembly version of the human genome reporting unique hits and allowing up to two mismatches. Within the 100-nt read length, we estimated that 90% of the sequences mapping to *Alu* elements were unambiguously mapped, given that this read length allows precise identification of the majority of the *Alu* elements (Umylny *et al*, 2007). For a selected set of genes (see Appendix Fig S2), comparison of various samples was done by normalizing expression levels to the total number of mapped reads and calculating the relative amounts. Read clusters showing the expression values normalized to the total number of mapped reads were calculated using Cufflinks (Trapnell *et al*, 2010). For annotation, the overlaps with genomic regions were evaluated based on Genomatix software suite (Genomatix, Munich, Germany). Clusters annotated as "exon-intron overlapping" comprise clusters overlapping exonic and intronic regions. After annotation, the clusters were compared to a primary transcripts (PT) database and re-grouped into PT when both exonic and intronic clusters corresponded to the same PT, or spliced transcripts when only exons were found.

A list of human *Alu* repeats was produced using the RepeatMasker track in the Table Browser ([www.genome.ucsc.edu](http://www.genome.ucsc.edu)) as well as a list of tRNAs. The average and normalized tRNA level was calculated for various samples (Appendix Fig S1) using the function "intersect" of the genome arithmetic suite bedtools (Quinlan & Hall, 2010). The same function was applied to list clusters overlapping with *Alu* repeats. The normalized expression (NE) values were used to classify the clusters and determine the highest enrichment in nucleoli or in the total RNA samples (see Appendix Table S2). For the graphical representation of the RNA-seq data, coverage files were produced with the Integrative Genomics Viewer toolbox and uploaded in the Integrative Genomics Viewer (Robinson *et al*, 2011). Multiple sequences alignment was performed using the alignment tool MultAlin (<http://multalin.toulouse.inra.fr>) (Corpet, 1988). Heatmaps were produced using the programs seqMINER (Ye *et al*, 2011) and ngs.plot (Shen *et al*, 2014).

## Data availability

RNA-seq data generated can be accessed via the EBI Array Express archive under the accession number E-MTAB-3460.

**Expanded View** for this article is available online:

<http://emboj.embopress.org>

## Acknowledgements

We are grateful to Joël Beaudouin, Ulrike Engel (Nikon Imaging Center, Heidelberg), David Ibberson (CellNetworks Deep Sequencing Core Facility, Heidelberg), Benjamin Schwalm and Claudio Flores for their help and advice; Gernot Längst, Sven Diederichs and Argyris Papantonis for helpful discussions; and Dirk Grimm, Nikolas Gunkel, Brian McStay, Aubry Miller and Mitsuru Okuwaki for providing reagents. This work was funded by a DKFZ young investigator grant to MC-H, the German Federal Ministry of Education and Research in the EU FP7 ERA-NET Plus program (grant 0315712A to KR) and the DFG (grants GR475/22-1 and SFB1036 to IG and grant SFB960 to AN).

## Author contributions

MC-H and KR conceived the project, coordinated the study and designed the experimental plan with help from IG, RV and AN. MC-H, TP, JS and RV conducted experiments and/or data analysis, and AN provided reagents. MC-H, KR, IG and RV wrote the manuscript.

## Conflict of interest

The authors declare that they have no conflict of interest.

## References

- Amin MA, Matsunaga S, Uchiyama S, Fukui K (2008) Depletion of nucleophosmin leads to distortion of nucleolar and nuclear structures in HeLa cells. *Biochem J* 415: 345–351
- Audas TE, Jacob MD, Lee S (2012) Immobilization of proteins in the nucleolus by ribosomal intergenic spacer noncoding RNA. *Mol Cell* 45: 147–157
- Batista PJ, Chang HY (2013) Long noncoding RNAs: cellular address codes in development and disease. *Cell* 152: 1298–1307
- Batzler MA, Deininger PL (2002) *Alu* repeats and human genomic diversity. *Nat Rev Genet* 3: 370–379
- Belancio VP, Roy-Engel AM, Deininger PL (2010) All y'all need to know 'bout retroelements in cancer. *Semin Cancer Biol* 20: 200–210
- Bergmann JH, Spector DL (2014) Long non-coding RNAs: modulators of nuclear structure and function. *Curr Opin Cell Biol* 26: 10–18
- Bierhoff H, Dammert MA, Brocks D, Dambacher S, Schotta G, Grummt I (2014) Quiescence-induced lncRNAs trigger H4K20 trimethylation and transcriptional silencing. *Mol Cell* 54: 675–682
- Boisvert F-M, van Koningsbruggen S, Navascués J, Lamond AI (2007) The multifunctional nucleolus. *Nat Rev Mol Cell Biol* 8: 574–585
- Boulon S, Westman BJ, Hutten S, Boisvert F-M, Lamond AI (2010) The nucleolus under stress. *Mol Cell* 40: 216–227
- Brangwynne CP, Mitchison TJ, Hyman AA (2011) Active liquid-like behavior of nucleoli determines their size and shape in *Xenopus laevis* oocytes. *Proc Natl Acad Sci USA* 108: 4334–4339
- Burger K, Mühl B, Harasim T, Rohrmoser M, Malamoussi A, Orban M, Kellner M, Gruber-Eber A, Kremmer E, Hölzel M, Eick D (2010) Chemotherapeutic drugs inhibit ribosome biogenesis at various levels. *J Biol Chem* 285: 12416–12425
- Busch H, Muramatsu M, Adams H, Steele WJ, Liau MC, Smetana K (1963) Isolation of nucleoli. *Exp Cell Res* 24(Suppl. 9): 150–163
- Callinan PA, Batzler MA (2006) Retrotransposable elements and human disease. *Genome Dyn* 1: 104–115
- Capshew CR, Dusenbury KL, Hundley HA (2012) Inverted *Alu* dsRNA structures do not affect localization but can alter translation efficiency of human mRNAs independent of RNA editing. *Nucleic Acids Res* 40: 8637–8645
- Carmo-Fonseca M, Mendes-Soares L, Campos I (2000) To be or not to be in the nucleolus. *Nat Cell Biol* 2: E107–E112
- Caudron-Herger M, Muller-Ott K, Mallm JP, Marth C, Schmidt U, Fejes-Toth K, Rippe K (2011) Coding RNAs with a non-coding function: maintenance of open chromatin structure. *Nucleus* 2: 410–424
- Caudron-Herger M, Rippe K (2012) Nuclear architecture by RNA. *Curr Opin Genet Dev* 22: 179–187
- Chafin DR, Guo H, Price DH (1995) Action of alpha-amanitin during pyrophosphorolysis and elongation by RNA polymerase II. *J Biol Chem* 270: 19114–19119
- Chaumeil J, Okamoto I, Guggiari M, Heard E (2002) Integrated kinetics of X chromosome inactivation in differentiating embryonic stem cells. *Cytogenet Genome Res* 99: 75–84
- Chen S, Seiler J, Santiago-Reichert M, Felbel K, Grummt I, Voit R (2013) Repression of RNA polymerase I upon stress is caused by inhibition of RNA-dependent deacetylation of PAF53 by SIRT7. *Mol Cell* 52: 303–313
- Chung I, Leonhardt H, Rippe K (2011) De novo assembly of a PML nuclear subcompartment occurs through multiple pathways and induces telomere elongation. *J Cell Sci* 124: 3603–3618
- Cong R, Das S, Ugrinova I, Kumar S, Mongelard F, Wong J, Bouvet P (2012) Interaction of nucleolin with ribosomal RNA genes and its role in RNA polymerase I transcription. *Nucleic Acids Res* 40: 9441–9454
- Corpet F (1988) Multiple sequence alignment with hierarchical clustering. *Nucleic Acids Res* 16: 10881–10890
- David-Pfeuty T, Nouvian-Dooghe Y, Sirri V, Roussel P, Hernandez-Verdun D (2001) Common and reversible regulation of wild-type p53 function and of ribosomal biogenesis by protein kinases in human cells. *Oncogene* 20: 5951–5963
- Defoiche J, Zhang Y, Lagneaux L, Pettengell R, Hegedus A, Willems L, Macallan DC (2009) Measurement of ribosomal RNA turnover in vivo by use of deuterium-labeled glucose. *Clin Chem* 55: 1824–1833
- Deininger P (2011) *Alu* elements: know the SINEs. *Genome Biol* 12: 236–247
- Deng Z, Norseen J, Wiedmer A, Riethman H, Lieberman PM (2009) TERRA RNA binding to TRF2 facilitates heterochromatin formation and ORC recruitment at telomeres. *Mol Cell* 35: 403–413
- Di Ruscio A, Ebralidze AK, Benoukrat T, Amabile G, Goff LA, Terragni J, Figueroa ME, De Figueiredo Pontes LL, Alberich-Jorda M, Zhang P, Wu M, D'Alo F, Melnick A, Leone G, Ebralidze KK, Pradhan S, Rinn JL, Tenen DG (2013) DNMT1-interacting RNAs block gene-specific DNA methylation. *Nature* 503: 371–376
- Dieci G, Fiorino G, Castelnuovo M, Teichmann M, Pagano A (2007) The expanding RNA polymerase III transcriptome. *Trends Gen* 23: 614–622
- Douset T, Wang C, Verheggen C, Chen D, Hernandez-Verdun D, Huang S (2000) Initiation of nucleolar assembly is independent of RNA polymerase I transcription. *Mol Biol Cell* 11: 2705–2717
- Eisenberg E, Levanon EY (2013) Human housekeeping genes, revisited. *Trends Genet* 29: 569–574
- Emmott E, Hiscox JA (2009) Nucleolar targeting: the hub of the matter. *EMBO Rep* 10: 231–238
- Fitzpatrick T, Huang S (2012) 3'-UTR-located inverted *Alu* repeats facilitate mRNA translational repression and stress granule accumulation. *Nucleus* 3: 359–369
- Ginisty H, Sicard H, Roger B, Bouvet P (1999) Structure and functions of nucleolin. *J Cell Sci* 112: 761–772
- Granick D (1975) Nucleolar necklaces in chick embryo fibroblast cells. II. Microscope observations of the effect of adenosine analogues on nucleolar necklace formation. *J Cell Biol* 65: 418–427

- Grimm D, Streetz KL, Jopling CL, Storm TA, Pandey K, Davis CR, Marion P, Salazar F, Kay MA (2006) Fatality in mice due to oversaturation of cellular microRNA/short hairpin RNA pathways. *Nature* 441: 537–541
- Grob A, Collieran C, McStay B (2014) Construction of synthetic nucleoli in human cells reveals how a major functional nuclear domain is formed and propagated through cell division. *Genes Dev* 28: 220–230
- Haaf T, Ward DC (1996) Inhibition of RNA polymerase II transcription causes chromatin decondensation, loss of nucleolar structure, and dispersion of chromosomal domains. *Exp Cell Res* 224: 163–173
- Han TW, Kato M, Xie S, Wu LC, Mirzaei H, Pei J, Chen M, Xie Y, Allen J, Xiao G, McKnight SL (2012) Cell-free formation of RNA granules: bound RNAs identify features and components of cellular assemblies. *Cell* 149: 768–779
- Hasler J, Strub K (2006) *Alu* elements as regulators of gene expression. *Nucleic Acids Res* 34: 5491–5497
- Hernandez-Verdun D, Roussel P, Thiry M, Sirri V, Lafontaine DL (2010) The nucleolus: structure/function relationship in RNA metabolism. *Wiley Interdiscip Rev RNA* 1: 415–431
- Hisaoka M, Ueshima S, Murano K, Nagata K, Okuwaki M (2010) Regulation of nucleolar chromatin by B23/nucleophosmin jointly depends upon its RNA binding activity and transcription factor UBF. *Mol Cell Biol* 30: 4952–4964
- Hisaoka M, Nagata K, Okuwaki M (2014) Intrinsically disordered regions of nucleophosmin/B23 regulate its RNA binding activity through their inter- and intra-molecular association. *Nucleic Acids Res* 42: 1180–1195
- Hoppe S, Bierhoff H, Cado I, Weber A, Tiebe M, Grummt I, Voit R (2009) AMP-activated protein kinase adapts rRNA synthesis to cellular energy supply. *Proc Natl Acad Sci USA* 106: 17781–17786
- Hutchinson JN, Ensminger AW, Clemson CM, Lynch CR, Lawrence JB, Chess A (2007) A screen for nuclear transcripts identifies two linked noncoding RNAs associated with SC35 splicing domains. *BMC Genom* 8: 39–54
- Hyman AA, Simons K (2012) Cell biology. Beyond oil and water—phase transitions in cells. *Science* 337: 1047–1049
- Ideue T, Hino K, Kitao S, Yokoi T, Hirose T (2009) Efficient oligonucleotide-mediated degradation of nuclear noncoding RNAs in mammalian cultured cells. *RNA* 15: 1578–1587
- Jacob MD, Audas TE, Mullineux S-T, Lee S (2012) Where no RNA polymerase has gone before: novel functional transcripts derived from the ribosomal intergenic spacer. *Nucleus* 3: 315–319
- Jacob MD, Audas TE, Uniacke J, Trinkle-Mulcahy L, Lee S (2013) Environmental cues induce a long noncoding RNA-dependent remodeling of the nucleolus. *Mol Biol Cell* 24: 2943–2953
- Jady BE, Ketele A, Kiss T (2012) Human intron-encoded *Alu* RNAs are processed and packaged into Wdr79-associated nucleoplasmic box H/ACA RNPs. *Genes Dev* 26: 1897–1910
- Jegou T, Chung I, Heuvelmann G, Wachsmuth M, Görisch SM, Greulich-Bode K, Boukamp P, Lichter P, Rippe K (2009) Dynamics of telomeres and promyelocytic leukemia nuclear bodies in a telomerase negative human cell line. *Mol Biol Cell* 20: 2070–2082
- Kaneko H, Dridi S, Tarallo V, Gelfand BD, Fowler BJ, Cho WG, Kleinman ME, Ponicsan SL, Hauswirth WW, Chiodo VA, Kariko K, Yoo JW, Lee DK, Hadziachmetovic M, Song Y, Misra S, Chaudhuri G, Buaas FW, Braun RE, Hinton DR et al (2011) DICER1 deficit induces *Alu* RNA toxicity in age-related macular degeneration. *Nature* 471: 325–330
- Laferte A, Favry E, Sentenac A, Riva M, Carles C, Chedin S (2006) The transcriptional activity of RNA polymerase I is a key determinant for the level of all ribosome components. *Genes Dev* 20: 2030–2040
- Lamaye F, Galliot S, Alibardi L, Lafontaine DLJ, Thiry M (2011) Nucleolar structure across evolution: the transition between bi- and tri-compartmentalized nucleoli lies within the class Reptilia. *J Struct Biol* 174: 352–359
- Langmead B, Trapnell C, Pop M, Salzberg SL (2009) Ultrafast and memory-efficient alignment of short DNA sequences to the human genome. *Genome Biol* 10: R25
- Li YP, Busch RK, Valdez BC, Busch H (1996) C23 interacts with B23, a putative nucleolar-localization-signal-binding protein. *Eur J Biochem* 237: 153–158
- Li TH, Schmid CW (2001) Differential stress induction of individual *Alu* loci: implications for transcription and retrotransposition. *Gene* 276: 135–141
- Liang XH, Crooke ST (2011) Depletion of key protein components of the RISC pathway impairs pre-ribosomal RNA processing. *Nucleic Acids Res* 39: 4875–4889
- Liu GE, Alkan C, Jiang L, Zhao S, Eichler EE (2009) Comparative analysis of *Alu* repeats in primate genomes. *Genome Res* 19: 876–885
- Mais C, Wright JE, José-Luis P, Raggett SL, McStay B (2005) UBF-binding site arrays form pseudo-NORs and sequester the RNA polymerase I transcription machinery. *Genes Dev* 19: 50–64
- Mao YS, Sunwoo H, Zhang B, Spector DL (2011) Direct visualization of the co-transcriptional assembly of a nuclear body by noncoding RNAs. *Nat Cell Biol* 13: 95–101
- Mattick JS, Mehler MF (2008) RNA editing, DNA recoding and the evolution of human cognition. *Trends Neurosci* 31: 227–233
- Mayer C, Schmitz K-M, Li J, Grummt I, Santoro R (2006) Intergenic transcripts regulate the epigenetic state of rRNA genes. *Mol Cell* 22: 351–361
- McKeown PC, Shaw PJ (2009) Chromatin: linking structure and function in the nucleolus. *Chromosoma* 118: 11–23
- Mercer TR, Mattick JS (2013) Understanding the regulatory and transcriptional complexity of the genome through structure. *Genome Res* 23: 1081–1088
- Nagai K, Oubridge C, Kuglstatter A, Menichelli E, Isel C, Jovine L (2003) Structure, function and evolution of the signal recognition particle. *EMBO J* 22: 3479–3485
- Nishihara H, Terai Y, Okada N (2002) Characterization of novel *Alu*- and tRNA-related SINEs from the tree shrew and evolutionary implications of their origins. *Mol Biol Evol* 19: 1964–1972
- Olson MO, Rivers ZM, Thompson BA, Kao WY, Case ST (1983) Interaction of nucleolar phosphoprotein C23 with cloned segments of rat ribosomal deoxyribonucleic acid. *Biochemistry* 22: 3345–3351
- Olson MO, Dunder M, Szebeni A (2000) The nucleolus: an old factory with unexpected capabilities. *Trends Cell Biol* 10: 189–196
- Olson MO (2004) Sensing cellular stress: another new function for the nucleolus? *Sci STKE* 224: pe10
- Pederson T (1998) The plurifunctional nucleolus. *Nucleic Acids Res* 26: 3871–3876
- Percipalle P, Fomproix N, Cavellan E, Voit R, Reimer G, Kruger T, Thyberg J, Scheer U, Grummt I, Farrants AK (2006) The chromatin remodelling complex WSTF-SNF2 h interacts with nuclear myosin 1 and has a role in RNA polymerase I transcription. *EMBO Rep* 7: 525–530
- Pontvianne F, Blevins T, Chandrasekhara C, Mozgova I, Hassel C, Pontes OM, Tucker S, Mokros P, Muchova V, Fajkus J, Pikaard CS (2013) Subnuclear partitioning of rRNA genes between the nucleolus and nucleoplasm reflects alternative epiallelic states. *Genes Dev* 27: 1545–1550
- Popov A, Smirnov E, Kovacic L, Raska O, Hagen G, Stixova L, Raska I (2013) Duration of the first steps of the human rRNA processing. *Nucleus* 4: 134–141

- Quinlan AR, Hall IM (2010) BEDTools: a flexible suite of utilities for comparing genomic features. *Bioinformatics* 26: 841–842
- Raska I, Ochs RL, Andrade LE, Chan EK, Burlingame R, Peebles C, Gruol D, Tan EM (1990) Association between the nucleolus and the coiled body. *J Struct Biol* 104: 120–127
- Reichow SL, Hama T, Ferré-D'Amaré AR, Varani G (2007) The structure and function of small nucleolar ribonucleoproteins. *Nucleic Acids Res* 35: 1452–1464
- Reynolds RC, Montgomery PO, Hughes B (1964) Nucleolar “caps” produced by actinomycin D. *Cancer Res* 24: 1269–1277
- Richard P, Darzacq X, Bertrand E, Jady BE, Verheggen C, Kiss T (2003) A common sequence motif determines the Cajal body-specific localization of box H/ACA scaRNAs. *EMBO J* 22: 4283–4293
- Robinson JT, Thorvaldsdóttir H, Winckler W, Guttman M, Lander ES, Getz G, Mesirov JP (2011) Integrative genomics viewer. *Nat Biotechnol* 29: 24–26
- Roeder RG, Rutter WJ (1970) Specific nucleolar and nucleoplasmic RNA polymerases. *Proc Natl Acad Sci USA* 65: 675–682
- Roy AM, West NC, Rao A, Adhikari P, Aleman C, Barnes AP, Deininger PL (2000) Upstream flanking sequences and transcription of SINES. *J Mol Biol* 302: 17–25
- Rubbi CP, Milner J (2003) Disruption of the nucleolus mediates stabilization of p53 in response to DNA damage and other stresses. *EMBO J* 22: 6068–6077
- Scheer U, Hügler B, Hazan R, Rose KM (1984) Drug-induced dispersal of transcribed rRNA genes and transcriptional products: immunolocalization and silver staining of different nucleolar components in rat cells treated with 5,6-dichloro-beta-D-ribofuranosylbenzimidazole. *J Cell Biol* 99: 672–679
- Schmidt U, Basyuk E, Robert MC, Yoshida M, Villemain JP, Auboeuf D, Aitken S, Bertrand E (2011) Real-time imaging of cotranscriptional splicing reveals a kinetic model that reduces noise: implications for alternative splicing regulation. *J Cell Biol* 193: 819–829
- Schneider CA, Rasband WS, Eliceiri KW (2012) NIH Image to ImageJ: 25 years of image analysis. *Nat Methods* 9: 671–675
- Shen L, Shao N, Liu X, Nestler E (2014) ngs.plot: quick mining and visualization of next-generation sequencing data by integrating genomic databases. *BMC Genom* 15: 284–297
- Shevtsov SP, Dundr M (2011) Nucleation of nuclear bodies by RNA. *Nat Cell Biol* 13: 167–173
- Singer SS, Mannel DN, Hehlhans T, Brosius J, Schmitz J (2004) From “junk” to gene: curriculum vitae of a primate receptor isoform gene. *J Mol Biol* 341: 883–886
- Sirri V, Hernandez-Verdun D, Roussel P (2002) Cyclin-dependent kinases govern formation and maintenance of the nucleolus. *J Cell Biol* 156: 969–981
- Sirri V, Urcuqui-Inchima S, Roussel P, Hernandez-Verdun D (2008) Nucleolus: the fascinating nuclear body. *Histochem Cell Biol* 129: 13–31
- Sullivan GJ, Bridger JM, Cuthbert AP, Newbold RF, Bickmore WA, McStay B (2001) Human acrocentric chromosomes with transcriptionally silent nucleolar organizer regions associate with nucleoli. *EMBO J* 20: 2867–2874
- Tajirishi MM, Tuteja R, Tuteja N (2011) Nucleolin: the most abundant multifunctional phosphoprotein of nucleolus. *Commun Integr Biol* 4: 267–275
- Trapnell C, Williams BA, Pertea G, Mortazavi A, Kwan G, van Baren MJ, Salzberg SL, Wold BJ, Pachter L (2010) Transcript assembly and quantification by RNA-Seq reveals unannotated transcripts and isoform switching during cell differentiation. *Nat Biotechnol* 28: 511–515
- Ugrinova I, Monier K, Ivaldi C, Thiry M, Storck S, Mongelard F, Bouvet P (2007) Inactivation of nucleolin leads to nucleolar disruption, cell cycle arrest and defects in centrosome duplication. *BMC Mol Biol* 8: 66–81
- Umylny B, Presting G, Efrid JT, Klimovitsky BI, Ward WS (2007) Most human *Alu* and murine B1 repeats are unique. *J Cell Biochem* 102: 110–121
- Weber SC, Brangwynne CP (2012) Getting RNA and protein in phase. *Cell* 149: 1188–1191
- Weinmann R, Roeder RG (1974) Role of DNA-dependent RNA polymerase 3 in the transcription of the tRNA and 5S RNA genes. *Proc Natl Acad Sci USA* 71: 1790–1794
- Wong LH, Brettingham-Moore KH, Chan L, Quach JM, Anderson MA, Northrop EL, Hannan R, Saffery R, Shaw ML, Williams E, Choo KHA (2007) Centromere RNA is a key component for the assembly of nucleoproteins at the nucleolus and centromere. *Genome Res* 17: 1146–1160
- Wu L, Pan J, Thoroddsen V, Wysong DR, Blackman RK, Bulawa CE, Gould AE, Ocaín TD, Dick LR, Errada P, Dorr PK, Parkinson T, Wood T, Kornitzer D, Weissman Z, Willis IM, McGovern K (2003) Novel small-molecule inhibitors of RNA polymerase III. *Eukaryot Cell* 2: 256–264
- Yang L, Lin C, Liu W, Zhang J, Ohgi KA, Grinstein JD, Dorrestein PC, Rosenfeld MG (2011) ncRNA- and Pc2 methylation-dependent gene relocation between nuclear structures mediates gene activation programs. *Cell* 147: 773–788
- Yang L, Lin C, Jin C, Yang JC, Tanasa B, Li W, Merkurjev D, Ohgi KA, Meng D, Zhang J, Evans CP, Rosenfeld MG (2013) lncRNA-dependent mechanisms of androgen-receptor-regulated gene activation programs. *Nature* 500: 598–602
- Yao H, Brick K, Evrard Y, Xiao T, Camerini-Otero RD, Felsenfeld G (2010) Mediation of CTCF transcriptional insulation by DEAD-box RNA-binding protein p68 and steroid receptor RNA activator SRA. *Genes Dev* 24: 2543–2555
- Ye T, Krebs AR, Choukrallah MA, Keime C, Plewniak F, Davidson I, Tora L (2011) seqMINER: an integrated ChIP-seq data interpretation platform. *Nucleic Acids Res* 39: e35
- Zarnack K, König J, Tajnik M, Martincorena I, Eustermann S, Stevant I, Reyes A, Anders S, Luscombe NM, Ule J (2013) Direct competition between hnRNP C and U2AF65 protects the transcriptome from the exonization of *Alu* elements. *Cell* 152: 453–466
- Zillner K, Filarsky M, Rachow K, Weinberger M, Längst G, Németh A (2013) Large-scale organization of ribosomal DNA chromatin is regulated by Tip5. *Nucleic Acids Res* 41: 5251–5262

# Appendix

## ***Alu* element-containing RNAs maintain nucleolar structure and function**

Maiwen Caudron-Herger, Teresa Pankert, Jeanette Seiler, Attila Nemeth, Renate Voit, Ingrid

Grummt and Karsten Rippe

### **Table of content**

Appendix Tables S1 to S5

Appendix Figures S1 to S9

## Appendix Tables

**Appendix Table S1. Distribution of transcripts in total, nucleoplasmic and nucleolar RNA.**

	genomic region	total RNA	nucleoplasmic RNA	nucleolar RNA
transcripts distribution (%)	primary transcripts (exon + intron)	70±14	89±1	42±1
	spliced transcripts (exon only)	26±15	8±3	32±2
	intron only	4±1	4±4	26±3
	intron only overlapping <i>Alu</i> repeats	1±2	2±1	10±2

**Appendix Table S2. List of read clusters overlapping intronic *Alu* elements found in the nucleolar RNA and the corresponding clusters found in nucleoplasmic and total RNA.**

NE indicates the normalized expression value for each cluster. Clusters are listed from the most enriched in the nucleolar RNA (top) to the most enriched in the nucleoplasmic and/or total RNA (bottom). The *Alu* repeat elements overlapping with those clusters are also listed. The table is provided as a separate Excel file (EMBOJ-2015-91458\_Appendix\_Table\_S2.xlsx).

**Appendix Table S3. Nucleolar-enriched *al*uRNA-containing clusters**

chr	start	end	NE nucleolar RNA	NE total RNA	strand	length	region*
chr1	10220812	10220975	826.20	14.60	+	163	Region_1
chr1	24842361	24842659	31.91	15.38	+	298	Region_2
chr1	62490955	62491452	10.81	8.16	+	497	Region_3
chr1	1.44E+08	1.44E+08	7334.69	47.93	+	149	
chr1	1.56E+08	1.56E+08	2284.79	69.33	-	122	
chr1	2.07E+08	2.07E+08	8074.64	13.35	+	150	
chr2	10931045	10931175	722.31	10.57	-	130	Region_4
chr2	17928824	17929014	85.96	3.06	-	190	Region_5
chr3	53342369	53342502	6076.67	52.00	-	133	Region_6
chr3	57887592	57887736	381.54	3.73	+	144	Region_7
chr5	1805384	1805768	21.00	4.16	+	384	
chr5	1.3E+08	1.3E+08	489.41	32.93	-	224	Region_8
chr5	1.34E+08	1.34E+08	721.33	29.82	+	129	Region_9
chr6	31746136	31746374	293.89	3.99	-	238	
chr6	99993898	99994040	435.77	19.46	-	142	Region_10
chr6	1.25E+08	1.25E+08	1843.40	43.17	+	129	Region_11
chr6	1.51E+08	1.51E+08	249.91	37.16	+	141	Region_12
chr6	1.51E+08	1.51E+08	108.62	73.31	+	209	
chr7	1068849	1069071	120.57	4.68	-	222	Region_13
chr8	1.24E+08	1.24E+08	30371.15	165.53	+	148	Region_14
chr9	95054566	95054871	4302.03	10.52	-	305	
chr9	1.3E+08	1.3E+08	58.22	29.55	-	709	Region_15
chr9	1.35E+08	1.35E+08	331.90	6.51	-	140	Region_16
chr10	1.04E+08	1.04E+08	661.39	35.40	-	122	Region_17
chr10	1.27E+08	1.27E+08	176.48	31.40	-	170	
chr11	73560978	73561107	1683.10	3.05	+	129	Region_18
chr11	93466262	93466929	374.35	40.96	-	667	
chr11	93467946	93468425	542.37	40.96	-	479	Region_19
chr14	31577361	31577475	2339.77	5.01	-	114	Region_20
chr14	59668192	59668491	12.84	3.04	+	299	
chr15	44112904	44113186	18.81	6.11	-	282	Region_21
chr15	60675435	60675834	19.33	5.23	-	399	Region_22
chr17	30525565	30525679	2658.83	687.80	+	114	Region_23
chr17	45739648	45739760	2767.31	3.06	+	112	
chr17	74041054	74041185	1371.99	613.05	-	131	
chr17	75085383	75085828	275.83	32.63	+	445	
chr18	12469997	12470134	811.83	3.73	-	137	Region_24
chr18	43705063	43705281	103.45	7.69	+	218	
chr19	1414038	1414704	3.20	3.07	+	666	Region_25
chr19	1636211	1636342	722.10	4.76	-	131	Region_26
chr19	1956418	1956567	513.26	30.19	+	149	
chr19	5140383	5140493	1658.66	3.07	+	110	
chr19	10672854	10673124	163.05	6.47	-	270	Region_27
chr19	13037137	13037464	58.67	24.44	-	327	Region_28
chr20	37055925	37058529	2251.72	59.20	-	2604	Region_29
chrX	19363525	19363662	3003.78	1405.53	+	137	Region_30
chrX	21862407	21862612	535.92	24.63	+	205	Region_31

\* Regions that were used for the alignment in Figure S2. NE indicates the normalized expression value for each cluster.

**Appendix Table S4. Sequences of DNA and RNA probes used in this study**

Sample	Sequence
<i>alu</i> RNA ASO 1	AGCGATTCTCCTGCCTCAGC
<i>alu</i> RNA ASO 2	GGCTCACTGCAACCGCCACC
<i>alu</i> RNA ASO 3	AGTAGCTGGGATTACAGGCA
control ASO	CCGTCAGCCAGTACTGCCTC
L1-repeat ASO	GGTTAGTTACATATGTATAC
7SL-RNA ASO	GGCATAGCGCACTACAGCCC
<i>alu</i> RNA LNA	AGCAATTCTCCTGCCTCAGC
B1 ASO - 1	TTTGTAGACCAGGCTGGCCT
B1 ASO - 2	ATCCGCCTGCCTCTGCCTCC
L1-repeat LNA	GCAGGTTAGTTACATATGTA
Northern blot <i>alu</i> RNA probe NB1	GGCTCACTGCAACCGCCACC
<i>alu</i> RNA FISH 1	GGGTTCAAGCGATTCTCCTGCCTCAGCCTCCCGAGTAG CTGGGACTACAG
<i>alu</i> RNA FISH 2	CGCCCGCCTCGGCCTCCCAAAGTGCTGGGATGACAGG CGTGAGCCACTGA
<i>alu</i> RNA FISH 1c	CTGTAGTCCCAGCTACTCGGGAGGCTGAGGCAGGAGA ATCGCTTGAACCC
<i>alu</i> RNA FISH 2c	TCAGTGGCTCACGCCTGTCATCCCAGCACTTTGGGAGG CCGAGGCCGGGCG
L1-repeat FISH	CATGGCACATGTATACATATGTAACCTGCACAATG TGCACATGTAC
Met tRNA FISH	GGTTTAGATCCATCGACCTCTGGGTTATGGGCCAGCA CGCTTCCGCTGC
Ala tRNA FISH	GGATCGAACCGAGGCCTCATAATGCAAAGCATGCGC TCTACCACTGAGC
RNA FISH, MS2 loops	GTCGACCTGCAGACATGGGTGATCCTCATGTTTTCTAG GCAATTA
Primer actin FWD	TATCCTGACCCTGAAGTACC
Primer actin REV	CTCGGTGAGCAGCACAGGG
Primer B1-1 FWD	AGGCCAGCCTGGTCTACAAA
Primer B1 REV	CGAGACAGGGTTTCTCTG
Primer B1-2 FWD	GGAGGCAGAGGCAGGCGGAT
forward <i>alu</i> RNA with MS2 loops	CTGGACTGACTTCATAGTTTAAACGTCAAGAGAAGGCC GGGCTCAGTGGCTCACGCCTGTCATCCCAGCACTTTG GGAGGCCGAGGCGGGCGGGTCACGAGGTCAAGAGAT CGAGACCATCCGGGCCGACACGGTGAACCCCGTCTC TATTAAGTATAAAGATTAGCTGGGCGTGGTGGCGGG CACCTGTAGTCCCAGCTACTCGGGAGGCTGAGGCAGG AGAATCGCTTGAACCCAGGGAGGTGGCGGTTGCAGTG AGCCGAGATCACACCATCGCACTCCAGCCTGGGCGAC

	AGAGCGAGAC
forward <i>aluRNA<sub>L</sub></i> with MS2 loops	CTGGACTGACTTCATAGTTTAAACGTCAAGAGAAGGCC GGGCTCAGTGGCTCACGCCTGTCATCCCAGCACTTTG GGAGGCCGAGGCCGGCGGGTCACGAGGTCAAGAGAT CGAGACCATCCGGGCCGACACGGTGAACCCCGTCTC T
forward <i>aluRNA<sub>R</sub></i> with MS2 loops	ATAAAAGTATAAAGATTAGCTGGGCGTGGTGGCGGGC ACCTGTAGTCCCAGCTACTCGGGAGGCTGAGGCAGGA GAATCGCTTGAACCCAGGGAGGTGGCGGTTGCAGTGA GCCGAGATCACACCATCGCACTCCAGCCTGGGCGACA GAGCGAGAC
CDV3 RNA with MS2 loops	GATGAGGTTTTCAAAAACCAGGCCCTTAACTTCAGCT AGACAACCAATATGCTGTGCTTGAAAATCAGAAAAGCA GCCACTCACAATACAATTAAGGAATGGGCTTTGCTAAC CCTTCTGAGGTAAGTACTGACTGCAGCTAACCACCACAA CAGCCATTCATCATCTGATCTCTGCTGGATCTACAGACA CCGATGCAGACCACTCGATTTTCATGACCGGCCCTATTG CACTATGGAAGTTAAAGTGTACGACTGCTCTATGCAT ATTGGATTTAGGGGAATTTTCATTGTTACATAAATGTGT GAACTAGTTTCAACAGTGTCTTTTCATATTTACTCTGCA AATACAAAAAACCAAAACCTGCAGCCAGTGGTCATTTT AAAATCTTTTTATGTTTCAGATACTGAGCCTTCATAAGGG TTGACTACCTCAGATTTGCTGCACTCATTGTGGACTTCA TGTGGATCACAACCTTCTGGATAAGAAGATTACAACCTATT AAGTGTGATGTGAACCTTGAACCCAGCTCTACTGGAT TCTTATCAGAAATCCTGCATAAAAAGTCAGCCATCTGG GTTCTGATCTGCTGTAAAAGATGAAGATTTAAGTGACCT TAATTAACCTGTCCTGTGCCCTACCCTTAAGGAATACTC TCTGTAGTAGGCTGTTGTTATATTAGACTTCCTGGAACA CACTGCTGAAAAGAACTGATGTGTTTCAGATCATCTGTGT AGGGCTGTGATTTGTAATTTAACTAATTGTATTCTGAG GTA
RepA RNA with MS2 loops	CACTCTTTTTCTATATTTTGCCCATCGGGGCTGCGGAT ACCTGGTTTTATTATTTTTCTTTGCCCAACGGGGCCGT GGATACCTGCCTTTTAATCTTTTTTATTGCCCCATCGG GGCCGCGGATACCTGCTTTTTATTTTTTTTCTTAGCC CATCGGGGTATCGGATACCTGCTGATTCCCTTCCCCTC TGAACCCCAACACTCTGGCCCATCGGGGTGACGGAT ATCTGCTTTTTAAAAATTTCTTTTTTTGGCCCATCGGG GCTTCGGATACCTGCTTTTTTTTTTTTTATTTTCTTGCC CATCGGGGCTCGGATACCTGCTTTAATTTTTGTTTTT TGCCCATCGGGGCCGCGGATACCTGCTTTGATTTTTT TTTTCATCGCCATCGGTGCTTTTTATGGATGAA
STARD7 RNA with MS2 loops	TACCAATCTTTATGTATTTATTCACACATTTGATAAAAAT GTCACAGTTAGGAGTGAAATCATTACAATGACATGAGT AACTGTACAGACAGACCCCAAGTGCAGAATCAAATTGC CCTAAGTCAGAACATGGAGCAACCGCAACTCCTTCGCA CTTGTGCATGTGTGTGCGCTCGCAGACGCACACACACA CACACATATTCTCTCTCTCTTTATGCACACATCCATCC ACATCCCAACAATTGCAGGTGCTAAGTTTGGACATAAC CCAGGGACTCTTCCCTGACTTCTGTCAGGTCTTGAAA GAAGAAGTAATAAATGAAAAGCAGCTGGGACTGCTCGA TGCATCTCTCTCTTCCAACAATGACGCGGAGAAGGCA AGACATACACTGGGGCAGCTACTTCTTGGCACAAAAA TGAACAGGCAACAAGAAGGTCAAGGAAGTGTTAAGTT

	<p>AGTCTCAGGTTTAAACCACTTTTCAACACCACAAAACAG  TAGCAAGCAGGAAAACAAAAACAAAAACAAAAACAAA  ACTCTGGCCCTCAAGACTCCAGAAAAAAGGGAAGGAG  GAGGATTTAAAACCTTGATCCCTATTATTCTAACAAATTG  CAGCATGACCATAAGCAAACCAGCTCGGTCAAACCTGA  CAGCATCAGATTGTGACCTTATCTGAACAGTGTAGTTCA  CTTTTATTTTGGCTCTGAAGAGAGGAAGAAAACTTTTT  AGAGGAACTTAATGGTAACATAAACCAAATCTCCACTGT  ATTAGTATTTGAGACAAGATTACATCTATGCATTACAC  AGCTTGTCTGTAGATCTGAGAGCTCCAAGGGAGTGGCC  CAGCCCCCATTCTCTGACTTTAGCCTTCTGAAAAGAA  CAAGTCAAACCTGAAATATGAAAAATAATACCTGAATCA  AAATGGTGTCTTCTATACAATCGGACTAGGGTAGAATCC  TGCTCAATTCCTCAACTCCTATTTGACACAAAAGTAAA  AAATTTTTAACTAAATTTAAATGTGATGTTTTGAGCATC  AAAAAGCTACTATCTAAAAGGATTAGTCTCCCAGTGTTT  TTGGTAAATGGGGAAGGTTAGGAAGGAGGCAATGATC  CAATGAATATAGAAGAACTGGCCGATTCACAGGAAACT  TGCTTTGGATAAGGTGAGTCAATGGGTGATATTGTGCA  GGCAGGGAGGGAAATTTCTTTGTACAAATTCATGTCCC  TGGCCAGGCATGGCCAGGAGTTCAAGACCAGCCTGG  GAAACAGAGTGAAACTCCATCTCTACTTAAAAAAAAAAAA  AAATTAATAATAACTTCATGTCTCTAGAGATAAAAAGCAA  GGTGCGGACAAGGCACTTAACATAGCCAAGTATCGTTC  ACACCCATTCACATCATGATTGTTACCAAGAGCACTCC  CAGTAGCCCCCTCATTGAGAGACTCAACTGGCCAACATA  TACTTTCCAGGTGGACCTGGAGAACTGAAGGAAATCCA  AAGCGCTGCACAATCGATGGTGGGATTTGGAATGTCAG  CAGAGGAACTACTCAGAGAAGCAAATGGAGGTCATCC  CCTTCTGGCCTGAGGTGAGAGGTTTGTTCAGATTAGC  TCAGTGAGATACCGAATTTCAAACAGTTGGCCTGAGA  ATATGACAACACTCCCACAAATGTAGCCTTCTTCTGTTT  TGATAAGAGCAATAAGGGCTCTGAATGAAATGGGACAT  CAGTTATTGAATTATCTTGCACTGGAAGTTACAGCAGAT  GCCTTCTAATACATGTGGCATGTCCCCCTTCTACAGCA  GAGTGATAACGGACTGAGACAGGGCTAGAAGCACCTT  GTCCCTTCTTATCCCAAAGCCTG</p>
<p>CORO1C RNA  with MS2 loops</p>	<p>TAATCAATGATTTTTATCTCTGAAAATGGAAGCAAGTGT  TTTGACAGAACACTATGGCCACTCTATAAGAGCCGACC  TAGGAGTAATCACTGTCTCTTCTGGGATGTCATGGC  TTAAAAAAAAAAAAAAAAAAGACAAAACAGGAAAATAA  TCCACAATGCTTTGGGCGCCTACTCTGAGCTTGGCTGG  GCATCCATTCATTAATAAGTCATAAGCTACAACTAAG  ATCAGGGTAACTTTCCCTTGGCCTCCTGCTTCTCTTTGA  ACCACATGCCCTACGGTGTTCACCACCATCAACA  TTACTTCATTAATTCGATATCAGAACCCTTAAACACTACT  GAATCTTAGACAAAAGGTCCTCAGCAGATTACATTGATA  AAGAAACAAATACAGATTTGAATATAAGTCATTGCCATT  ATTGTTTTCTTACATCTCATGATCCACTTCAATATTA  CACATACATACACACACAAAACCACATCAAACATTCA  GATGCCCTGAAATTGTGGAGACAGCACTCCAGTATTG  GCTGGATAAGAACATGGTCCTTTTTCTACACGGACATTA  CTCCAAGTTCGGCTGTCACCACACTCTGCCCTCACCCT  GGCTCCCTGCATACAGACGTTTCCAGCCAGTCCCATGC  CCACACCAGCACGAGCATGTGCAAGAATTCCCTTCGTG</p>

	<p>GTCCCAATGGCACTACACATTTACGTTCAATCACAGA  CAGCCCTTCCAAAACAGAGGCTCCTTAAATCTTGTTTC  CAAGCATGCACTATAAGAACTGGAAACGGGGCAAAGT  TCCAGCTAACCGAGGAATGAACAGGTGACCAGAGCTC  AGTCTCTGGCCCCCTCCGAGTCCGGGGAGCCTCTGTG  CTTTGACGCAGCCTTGGTGAGAGATGGAGAGGCAGGG  CAGGTTAGTTGTGCGGAGGGACATGTTTGTATGCATTA  AAGCTACAGCAGAGGTCTGTGCTCCTGTTTCTGCTTCA  CTCTCTATCATTCTCCTCAGTCTCAATACTCATTCAATC  GCACCCTCTGGCCTTGTCTTAGCTTAATGTGGTTAGAG  CTAAAAGGCAGGAAGGAAAGAAGGAATGGCTGGGGGA  GCCCTGAGAGAGGTGCGCAGCACATGTGAGGAAGAGGG  TAGAGCAGGAGCTTTGTTGGTGGAAAGGAGAGCCACTT  CCTCCTCCAACACAGCATGGGGACAGCACAGGGAAAC  AGGATCACCCAGGGCAAATACCCCTCTCCACATGCCCA  CATTTTTAGTCCCCACCACTGTAAGAGCTGGGCA  AGCTGCTGAAAAGGGCAAGAAGGAACACTCAGCAGTA  CACGTCTTCTGTCTGGGCACCCTTGTCAAGTATTGA  CCAAAACCTGAAACATGATGTTTAAAGTGATGAATGCAA  TATGATCCTAGGTGTGTAACAACTGCAGAAACACATG  CTAGTTTGGGTTAGATTATAATCATCTGAAGCACAGGAT  AACCGAGAAGCAAATTCATTCTGGTACAAACACCCA  ATTTCTAGAAAAGAGAAAAGGAAAAGAAGAAATACGACG  TGAGCTTTTTTGTATCAGAAGACTCCATGAAATGAGAGC  GGTGGTAATATGAATCCACGTGATTTTTCAAGTCTTCT  GTTGTACAGTCATCAAATGACCAGGTTTGTGCTGCA  AAGGAGCCAGCACCATGTGGCTACTGCTTTGATTGTTT  TCAGATGAATGTTTATACAAAATAATATCTTATCTTCATT  TAGTTTATAAACATACACAGTGCTGTCCCTTTCAAATTA  AGGAAAAAAAAACCACACACACAAATACTGCAAAGTAGC  AAAATACAAAGGAAAACAAAGCTACTTTTGGTTTTGGCA  ACATTAAGAAAGAAAGAAATATAAAAAGCAATGTGGCAT  TGGTCCCTATTCATTAAGAAAGGGTACTTGGGCA  CGACACAATCAGAATTAGTTTGTCTAAAATTCAGAG  TATCTGGGATTTTAAAAGTAGCACTTTTTAAAAGTTCA  ACAAGTCACATAACACTTAAAACATCAAAAAGCTTTCT  GATAAAAAGCTCAGCTTTTAAATCACGTTTTGTTTCTGC  AAATTTGGGAGACAAATTGAGTTCTTACTGGAATGTGG  CCTATCGCTGGTTGACAAATCTGAAATGGAATGTCTCC  AAATGGCAGTGCCTCCCTTCCGCCCTCCCTAGGACCA  CACCAATAACCAGCTCCAAGCACAGTTCTTGCTCCC  ATTTTTCTGTAGGGGTGGGGGTGGGACCT</p>
forward <i>alu</i> RNA template for T7 <i>in vitro</i> transcription	<p>TAATACGACTCACTATAGGGCTGGACTGACTTCATAGTT  TAAACGTCAAGAGAAGGCCGGGCTCAGTGGCTCACGC  CTGTATCCAGCACTTTGGGAGGCCGAGGCGGGCGG  GTCACGAGGTCAAGAGATCGAGACCATCCGGGCGGAC  ACGGTCAAACCCCGTCTCTATTAAGTATAAGATTAG  CTGGGCGTGGTGGCGGGCACCTGTAGTCCAGCTACT  CGGGAGGCTGAGGCAGGAGAATCGCTTGAACCCAGGG  AGGTGGCGGTTGCAGTGAGCCGAGATCACACCATCGC  ACTCCAGCCTGGGCGACAGAGCGAGAC</p>
reverse <i>alu</i> RNA template for T7 <i>in vitro</i> transcription	<p>TAATACGACTCACTATAGGGGTCTCGCTCTGTCGCCCA  GGCTGGAGTGCGATGGTGTGATCTCGGCTCACTGCAA  CCGCCACCTCCCTGGGTTCAAGCGATTCTCCTGCCTCA  GCCTCCCGAGTAGCTGGGACTACAGGTGCCCGCCACC</p>

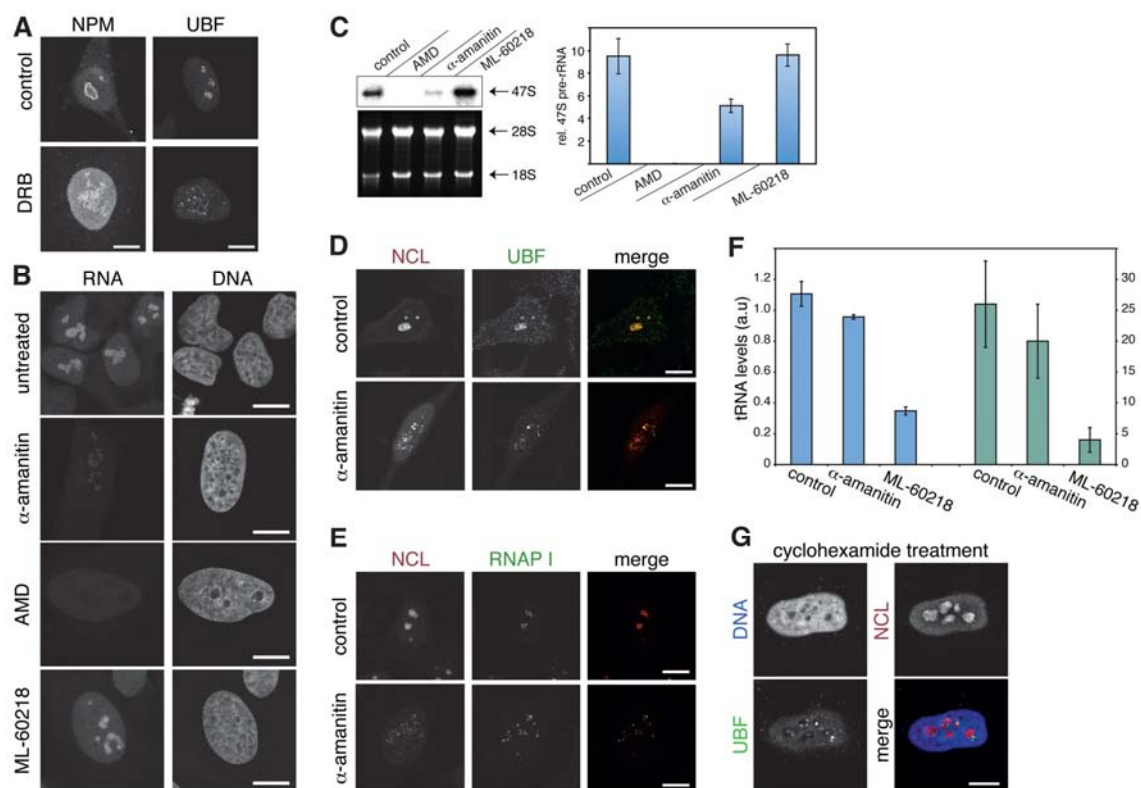
	ACGCCCAGCTAATCTTTATACTTTTAATAGAGACGGGGT TTCACCGTGTCTGGCCCCGGATGGTCTCGATCTCTTGACC TCGTGACCCGCCCGCCTCGGCCTCCCAAAGTGCTGGG ATGACAGGCGTGAGCCACTGAGCCCGGCCTTCTCTTG ACGTTTAAACTATGAAGTCAGTCCAG
RNA <sub>L</sub> template for T7 <i>in vitro</i> transcription	TAATACGACTCACTATAGGGCTGGACTGACTTCATAGTT TAAACGTCAAGAGAAGGCCGGGCTCAGTGGCTCACGC CTGTCATCCCAGCACTTTGGGAGGCCGAGGCGGGCGG GTCACGAGGTCAAGAGATCGAGACCATCCGGGGCCGAC ACGGTGAAACCCCGTCTCT
RNA <sub>R</sub> template for T7 <i>in vitro</i> transcription	TAATACGACTCACTATAGGGATTAAGTATAAAGATTA GCTGGGCGTGGTGGCGGGCACCTGTAGTCCCAGCTAC TCGGGAGGCTGAGGCAGGAGAATCGCTTGAACCCAGG GAGGTGGCGGTTGCAGTGAGCCGAGATCACACCATCG CACTCCAGCCTGGGCGACAGAGCGAGAC
CDV3a template for T7 <i>in vitro</i> transcription	TAATACGACTCACTATAGGGAAATTCAAGGACGAATATT TTCAAAAACCTAGTGAAGAAGAAATATTTACTGATTAC ATTTCTTTCCCTTAG
CDV3b template for T7 <i>in vitro</i> transcription	TAATACGACTCACTATAGGGGACCACCAGAAATCTACA GTGATACACAGTTCCCATCCCTGCAGTCAACTGCCAAG CATGTAGAAAGCCGGAA
L1-repeat template for T7 <i>in vitro</i> transcription	TAATACGACTCACTATAGGGGACAGAGGCATTATTCAC AATAGCAAAGACTTCGAACCAACCCAAATGTCCAACAA TGATAGACTGGATTAAGAAAATGTGGCACATATACACC ATGGAATACTATGCAGCCATAAAAAATGATGAGTTCATG TCCTTTGTAGGGACATGGATGAAATTGGAAATCATCATT CTCAGTAACTATCGCAAGAACAACAAAAACCAAACACCG CATATTCTCATAGGTGGGAACTGAACAATGAGATCACA TGGTCACAGGAAGGGGAATATCACACTCTGGGAACTGT GGTGGGGTGGGGGGAGGGGGGAGGGGATAGCATTGGG AGATATACCTAATGGTAGATGACGAGTTAGTGGGTGCA GCACACCAGCATGGCACATGTATACATATGTAACCTAAC CTGCACAATGTGCACATGTACGTAAAACCTTAAAG

**Appendix Table S5. Summary of reads obtained from RNA-seq**

<b>sample</b>	<b>read length</b>	<b># reads</b>	<b># uniquely mapped</b>	<b>% mapped*</b>
total RNA	36	44748728	17509543	82
nucleolar RNA	36	39049758	15077407	91
total RNA	100	64020509	35257382	73
nucleoplasmic RNA	100	72257683	26527408	68
nucleolar RNA	100	60301513	11002830	64
total RNA, control	100	45478612	21587838	65
total RNA, $\alpha$ -amanitin	100	42072870	19739852	65
total RNA, ML-60218	100	45270772	21404418	77
total RNA, control	100	62902322	34570403	87
total RNA, $\alpha$ -amanitin	100	64700649	33350538	82
total RNA, ML-60218	100	41871486	21033049	67
total RNA, mock	100	53274853	26363971	73
total RNA, <i>alu</i> RNA ASO	100	55449460	27732908	77
total RNA, control ASO	100	51555714	28641577	77

\* including multiple mapped reads and rRNA reads.

## Appendix Figures



### Appendix Figure S1. Effects of drug treatment on nucleolar structure and function.

A. CLSM images of HeLa cells treated with DRB and of untreated control. The nucleolar marker proteins NPM and UBF were visualized by immunofluorescence with antibodies specific to NPM or UBF.

B. CLSM images of HeLa cells after treatment with the indicated drugs. Nascent RNA was pulse labeled with EU, and DNA was stained with DAPI.

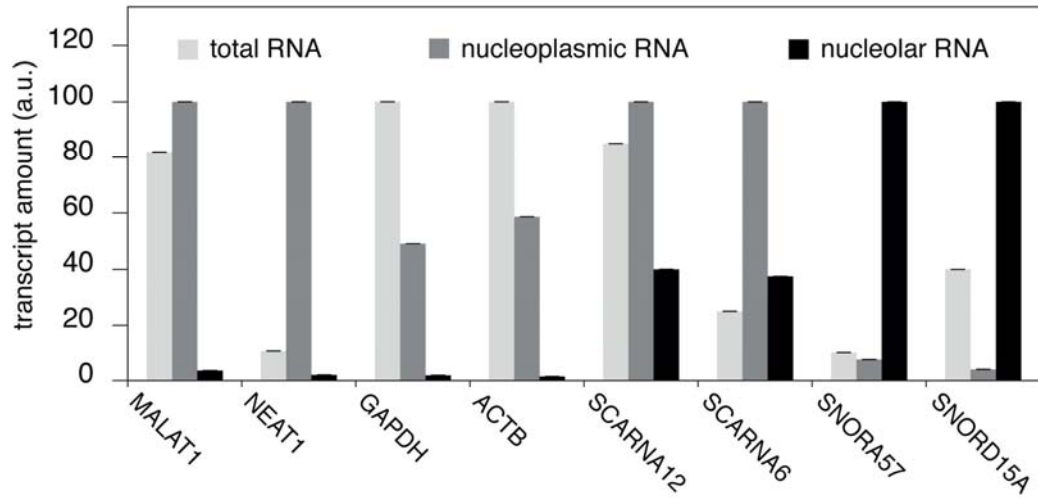
C. Northern blot showing rRNA levels in untreated-, AMD-,  $\alpha$ -amanitin- and ML-60218-treated HeLa cells (left). The 47S pre-rRNA has a very short half-life time in the range of minutes (Popov et al., 2013) as compared to 18S and 28S that are stable for days (Defoiche et al., 2009). Accordingly, 47S steady-state levels reflect the rRNA synthesis rate. For quantification, samples were normalized to 18S rRNA as determined by RT-qPCR. Error bars represent the standard deviation ( $n = 6$ ).

D. CLSM images of HeLa cells treated with  $\alpha$ -amanitin. The localization of NCL (red) and UBF (green) was detected by immunofluorescence.

E. Same as in panel D but for NCL (red) and Pol I (green).

F. Tyrosine tRNA levels normalized to 18S rRNA as measured by RT-qPCR (left y-axis, blue) or RNA-seq (right y-axis, green) in untreated (control),  $\alpha$ -amanitin- or ML-60218-treated total RNA samples ( $n = 2$ ).

G. Distribution of DNA (blue), UBF (green) and NCL (red) in HeLa cells treated with cycloheximide for 5 hours and visualized by CLSM. Scale bars, 10  $\mu$ m.



**Appendix Figure S2. Distribution of selected transcripts in total, nucleoplasmic and nucleolar RNA fractions.**

The relative amount of the indicated transcripts within the total, nucleoplasmic and nucleolar RNA fractions is plotted. Scale bars, 95% confidence interval (95% CI).



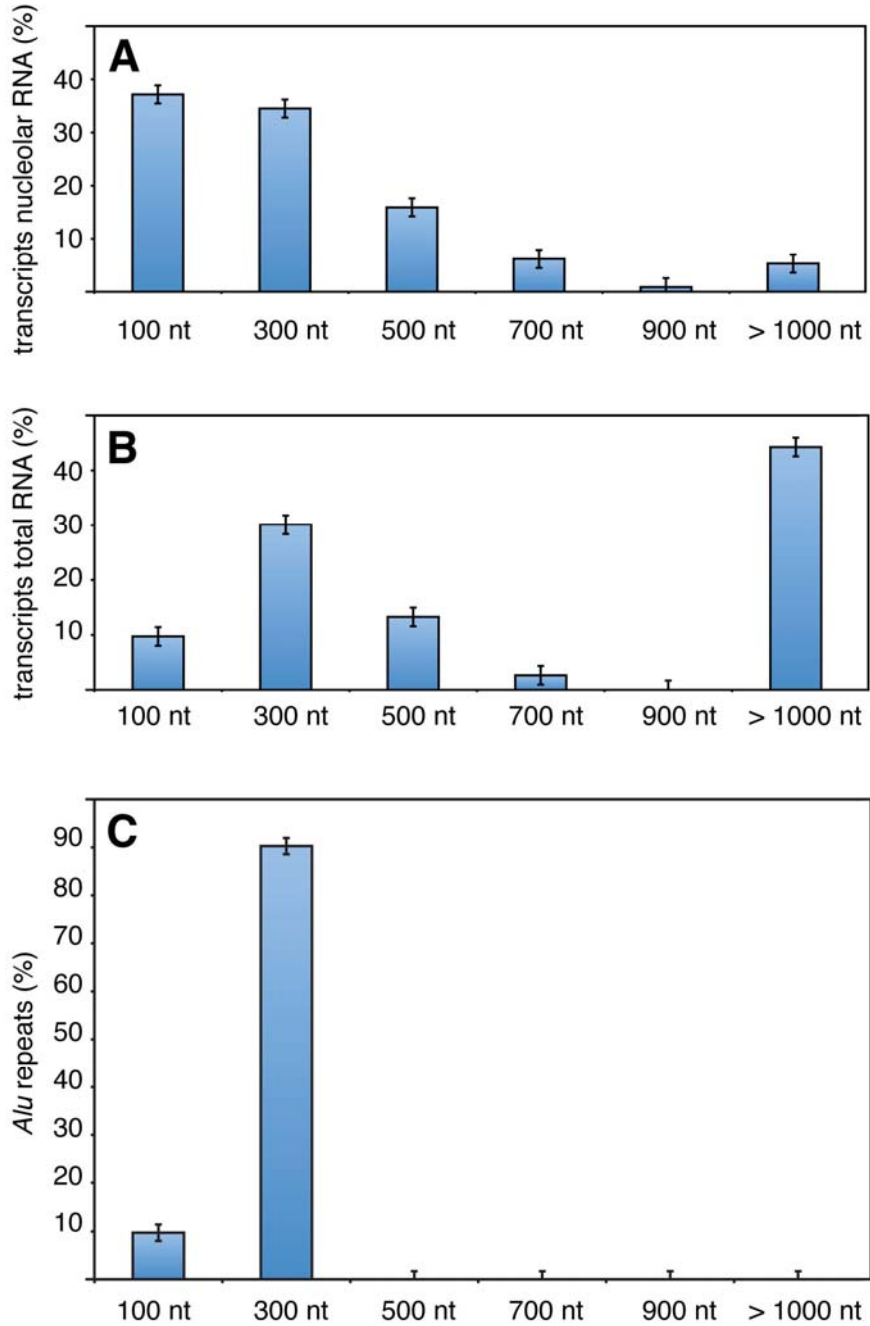
```

Region_7 -----AGAT CATGCCACCA CACTCCAGCC TG-G
Region_14 -----GGAT TGTGCCACTG TGCTCCAGCC TG-GGTGACA G
Region_30 -----AGAT CGTGCCATG CACTACGGCC T
Region_26 -----AGAT CGCACCCTG C
Region_23 AAAAAAAGGC TGGGCATGAT GGCTTATGCC TGTAAATCCA G-----CA CTTTGGGAGG C
Region_11 -----AGAT CACACCCTG CA
Region_24 -----TGAT TGCACCA
Region_2 -----AGAT TGCGCCAGCG TACTCCAGCC TG-GGCAACA GAGCGAGACT CAGTCTCAAG AAAAAAAAAA G--AAAGAA GAAACA
Region_3 -----AGGT AGTG
Region_25 -----AGAT CGGCCACTA CACTCC
Region_29 -----TGAC CATGCCACTG CACTC-AGCC TG-GGCAACA GAGTGAGACC CTGTCTCAAG AAAGAAAAAC GAGAAAGGGA GAGTCCCTCC ACTGTAAGGA GATCGGGTTC ATTACATTTT GGGGTGTTGG
Region_15 -----AGAT TGTGCCACTG CACTCCAGCC TG-GGTAACA G--TGAGACT CCGTCTCAA AAAAAAAAAA ---AAAGTGC CATGTAGTCC -CTGTGTGGG G--CAGGCC CAATCAGT-- -GCATGTGGG
Region_19 -----TGAT GGCACCCTG TACTCCAGCC TG-AGTAACA AAGACAGACC CTGTCTCTTA AGAAAAAAG
Region_22
Region_21
Region_28 -----AGAT CATGCCACTG CA
Region_27
Region_13
Region_31 -----TGAC CGTGCCACTG CACTCCAAC TG-GGTGA
Region_5 -----AGAT TGTGCCACTG CA
Region_8 -----AGAT CATGCCATG CACTAC
Region_4
Region_20 -----AGAT
Region_9 -----CAAT TGCACAAC TG CACTACAACC TG
Region_6 -----TTAT TCTGCCACTG CACTCCAGC
Region_17 -----TGGT GGCACCCT
Consensus agat .g.gccactg .....

```

**Appendix Figure S3. Sequence alignment of nucleolar-enriched *alu* RNAs.**

*Alu* element-containing RNAs (regions 1 to 31 from Table S2) enriched in the nucleolar RNA preparation over total RNA were aligned to derive a consensus sequence for nucleolar *alu* RNA (bottom line in the alignment). The degree of similarity to the consensus sequence is indicated by different colors: high, red; moderate, blue; neutral, black.

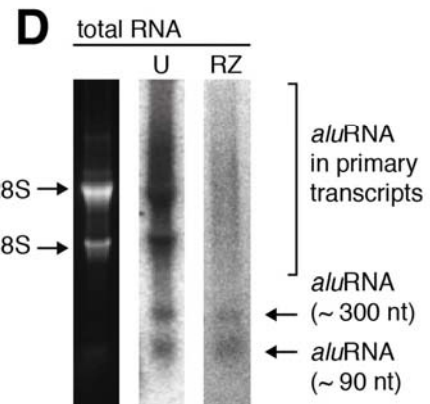
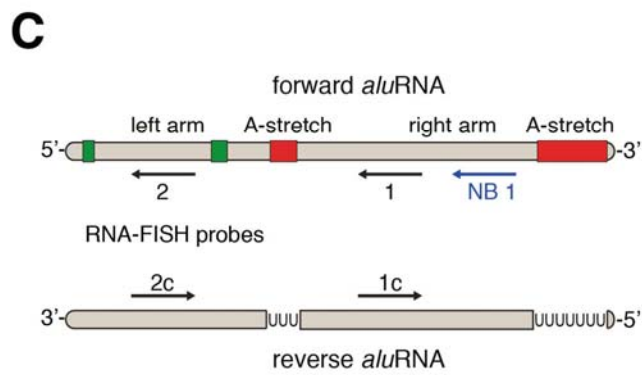
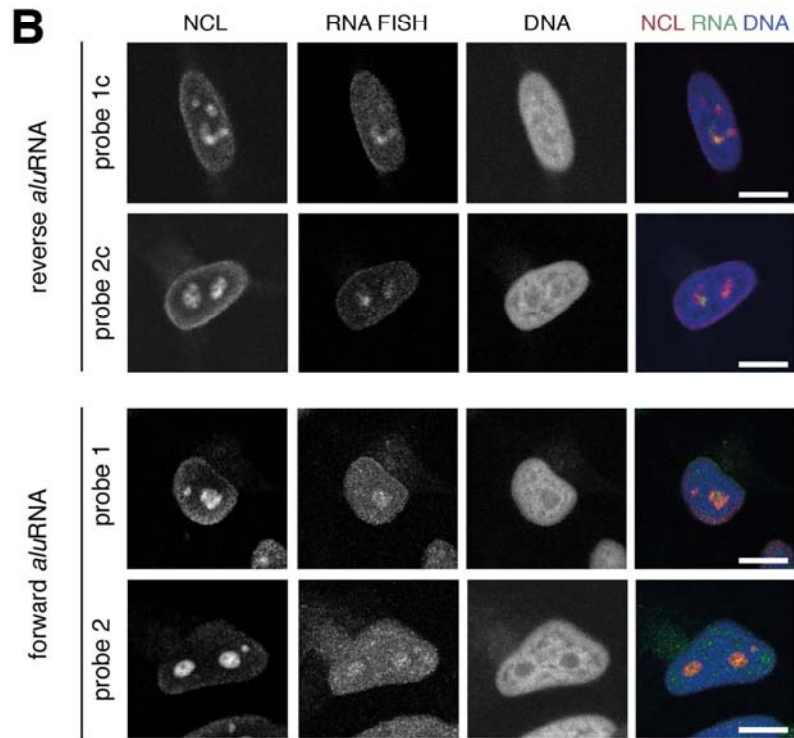
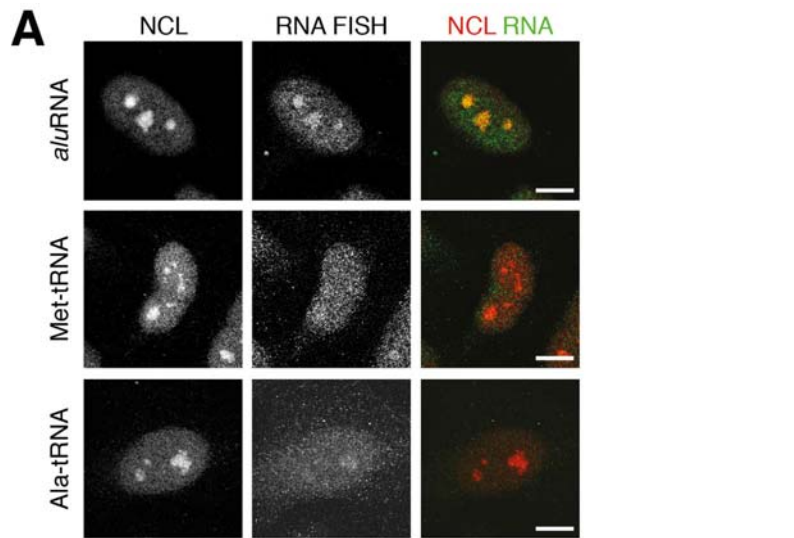


**Appendix Figure S4. Length distribution of *Alu* repeat-containing RNA transcripts from RNA-seq and corresponding genomic *Alu* elements.**

A. Length distribution of *Alu* repeat-containing nucleolar RNA sequences.

B. Length distribution of *Alu* repeat-containing total RNA sequences.

C. Length distribution of *Alu* element in the genome, which overlap with the RNA sequences from panel A and B.



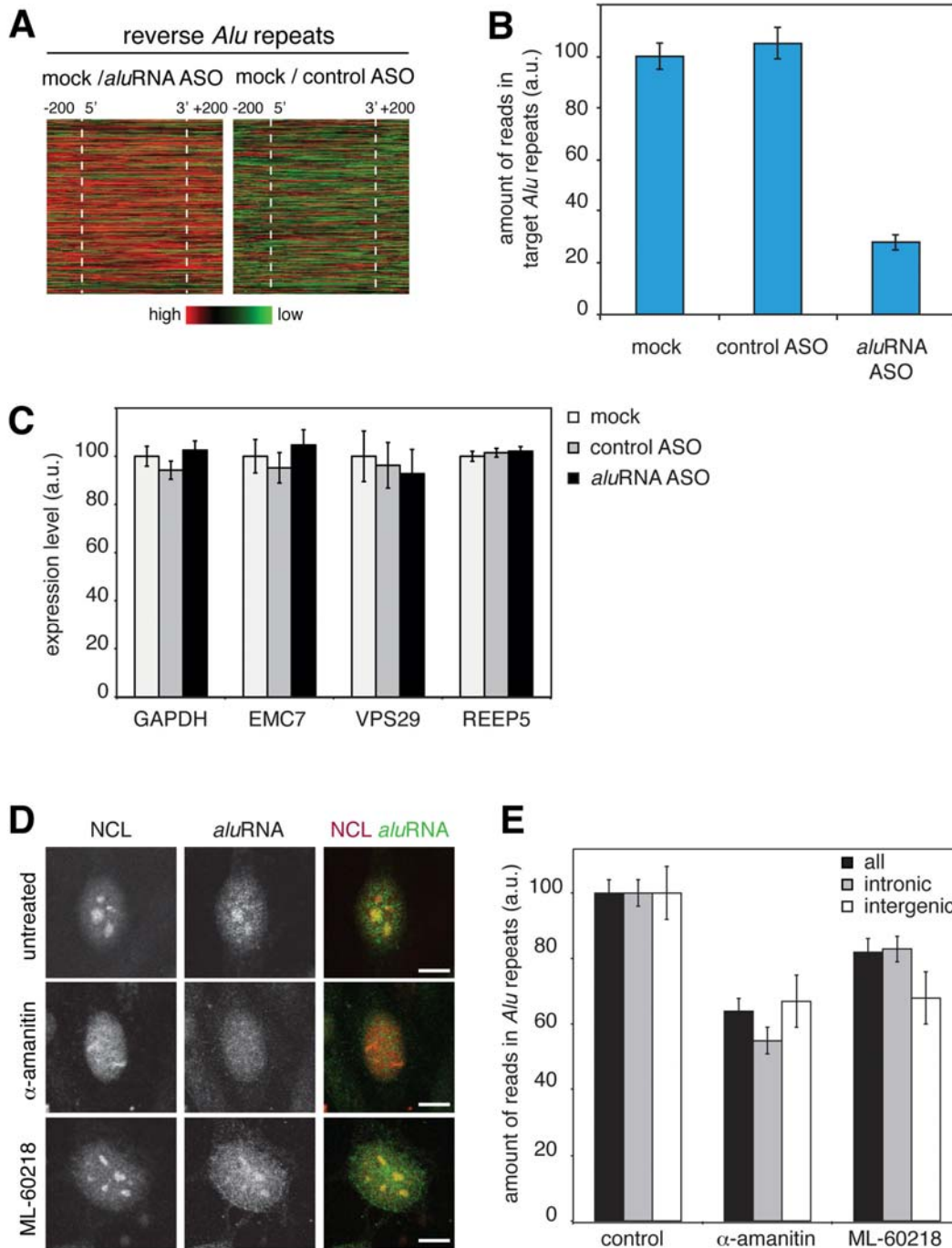
**Appendix Figure S5. Detection of *alu*RNAs in nucleoli and in total RNA.**

A. CLSM images of RNA-FISH analysis in HeLa cells using probes specific to forward *alu*RNA, methionine (Met-tRNA) and alanine (Ala-tRNA) tRNA sequences in HeLa cells. There is a weak signal in the nucleoli for the two tRNAs, which is in agreement with a small number of sequencing reads matching tRNA sequences found in the nucleolar fraction. The image intensity for the three RNA FISH images was normalized to the same nuclear intensity.

B. CLSM images of RNA-FISH against forward or reverse *alu*RNA sequences in HeLa cells. Color coding of merge image: RNA-FISH, green; NCL immunofluorescence, red; DNA (DAPI staining), blue. Scale bars, 10  $\mu$ m.

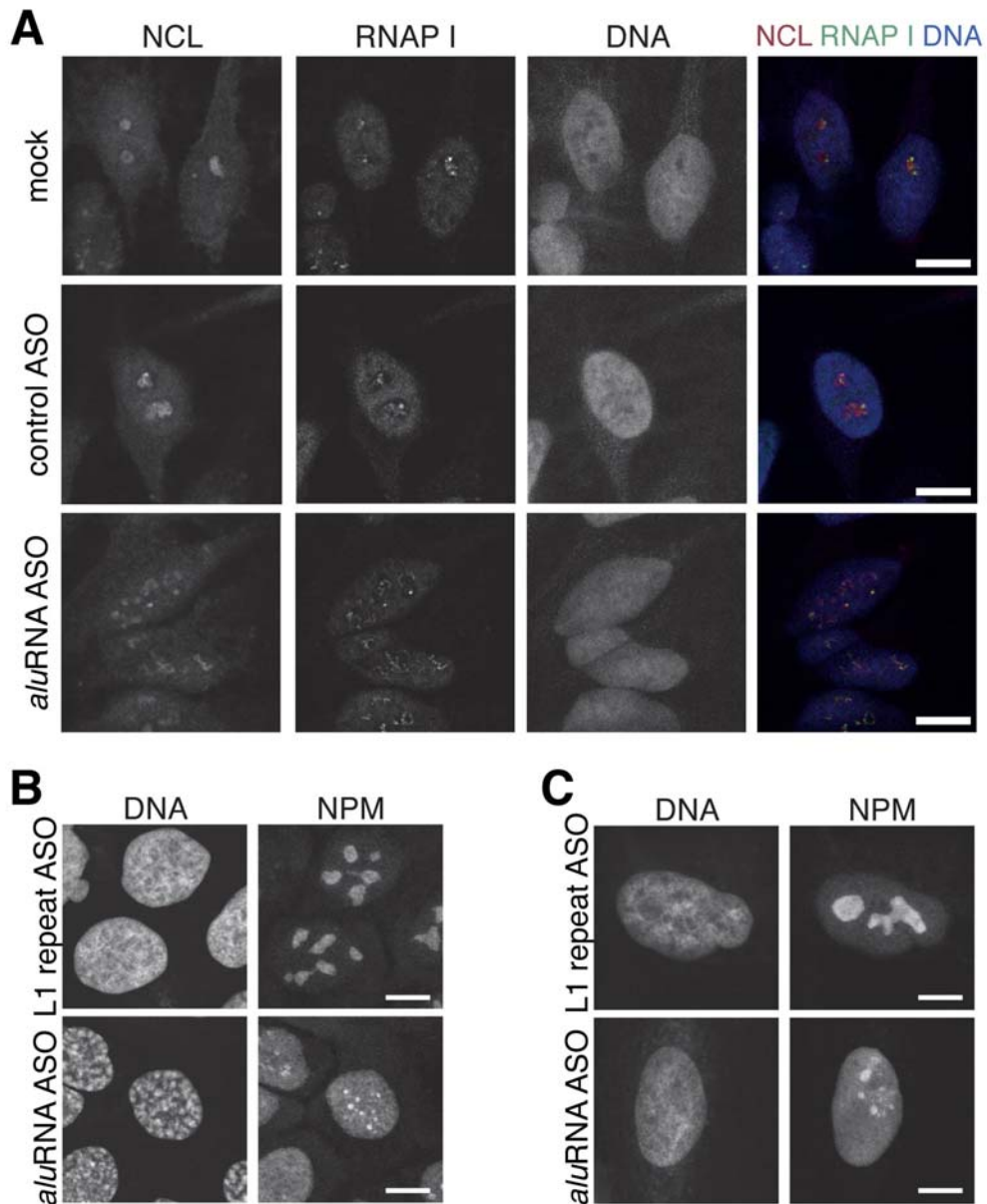
C. Scheme showing target sites of different RNA-FISH probes (1, 2, 1c and 2c, black arrows) and northern blot probe (NB 1, blue arrow) within a forward (top) or reverse (bottom) *Alu* repeat RNA sequence.

D. Northern blot analysis of purified total RNA probed with a sequence (NB1, see Appendix Table S4 and panel C) that targets the right arm of an *Alu* element. The bracket marks long primary transcripts with embedded *alu*RNA sequences. The position of the 300 nt length RNA was calculated according to co-migration of 7SL RNA and the position of the ~90 nt length RNA according to co-migration of tyrosine tRNA. In the lane labeled with RZ, a RiboZero-treated RNA sample was loaded, lane U an untreated sample. The position of 28S and 18S rRNA was detected by ethidium bromide staining of the untreated RNA sample.



**Appendix Figure S6. *aluRNA* levels are reduced after *aluRNA* ASO-mediated depletion and  $\alpha$ -amanitin treatment.**

- A. Heatmaps of read ratios obtained from total RNA sequencing of HeLa cells. Mock (transfection reagent only) ratio to *alu*RNA-ASO or control-ASO transfected cells. Colors indicate high (red) to low (green) read ratios.
- B. Graph showing the amount of reads corresponding to *Alu* repeats that were targeted by the *alu*RNA ASO (n = 3737). Cells were treated with ASO as indicated.
- C. Graph showing the expression levels of house keeping genes in ASO-treated cells as in panel B.
- D. CLSM images of HeLa cells treated as indicated. The distribution of NCL (immunofluorescence) and *alu*RNA (RNA FISH) are shown. Color-coding in the merge images: red, NCL and green, *alu*RNA. Scale bars, 10  $\mu$ m.
- E. Graph showing the amount of reads corresponding to all (n = 330 000), intronic (n = 250 000) or intergenic (n = 70 000) *Alu* repeats position. Cells were treated as indicated.



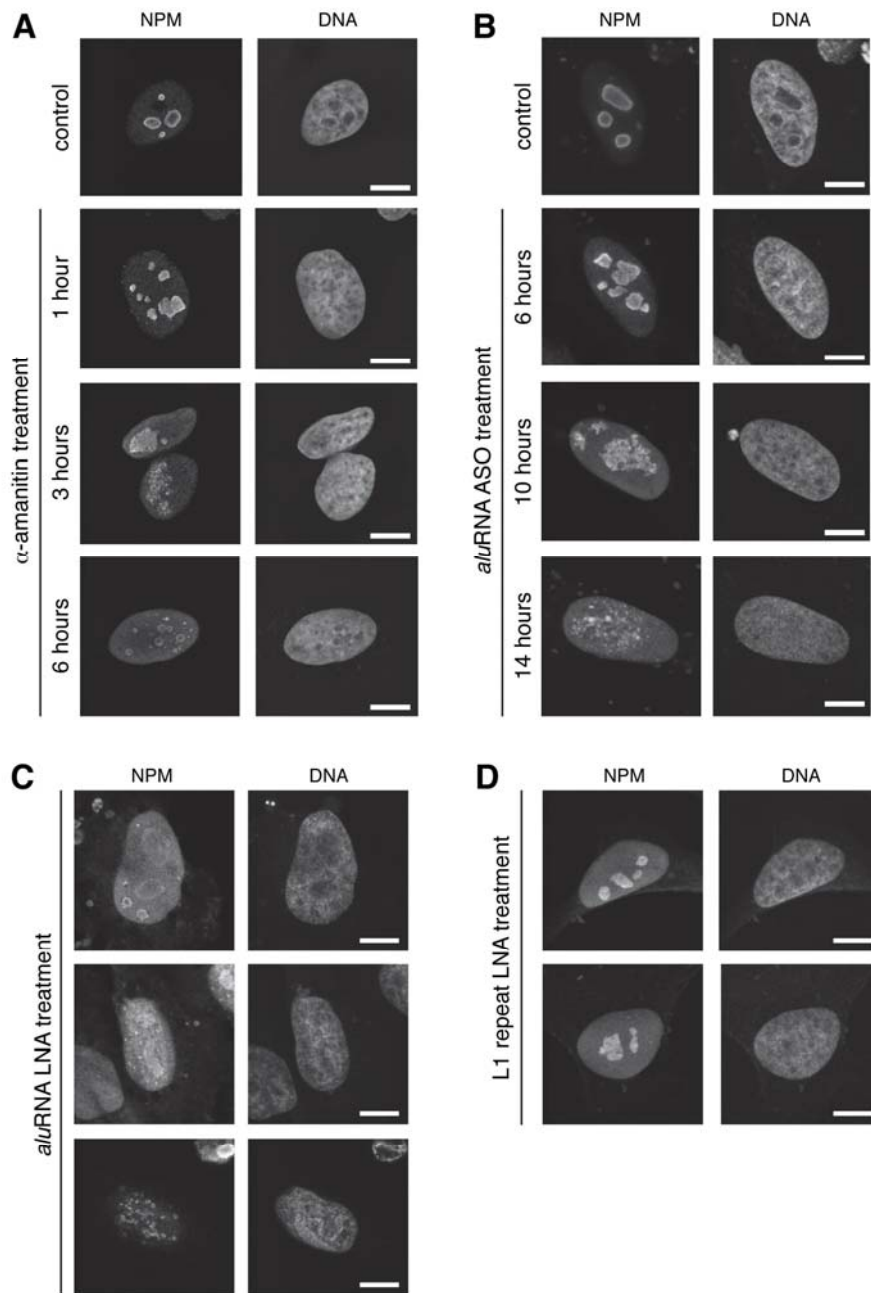
**Appendix Figure S7. Antisense oligonucleotides against *aluRNA* disrupt the nucleolar structure in different human cell types.**

A. CLSM images of HeLa cells treated with the indicated ASO. Nucleoli were visualized by immunofluorescence of NCL (red), Pol I (green), DNA was stained with DAPI.

B. CLSM images of human keratinocytes treated with the indicated ASO. Nucleoli were visualized by immunofluorescence of NPM (red), DNA was stained with DAPI.

C. CLSM images of human fibroblasts treated with the indicated ASO. Nucleoli were visualized by immunofluorescence of NPM (red), DNA was stained with DAPI.

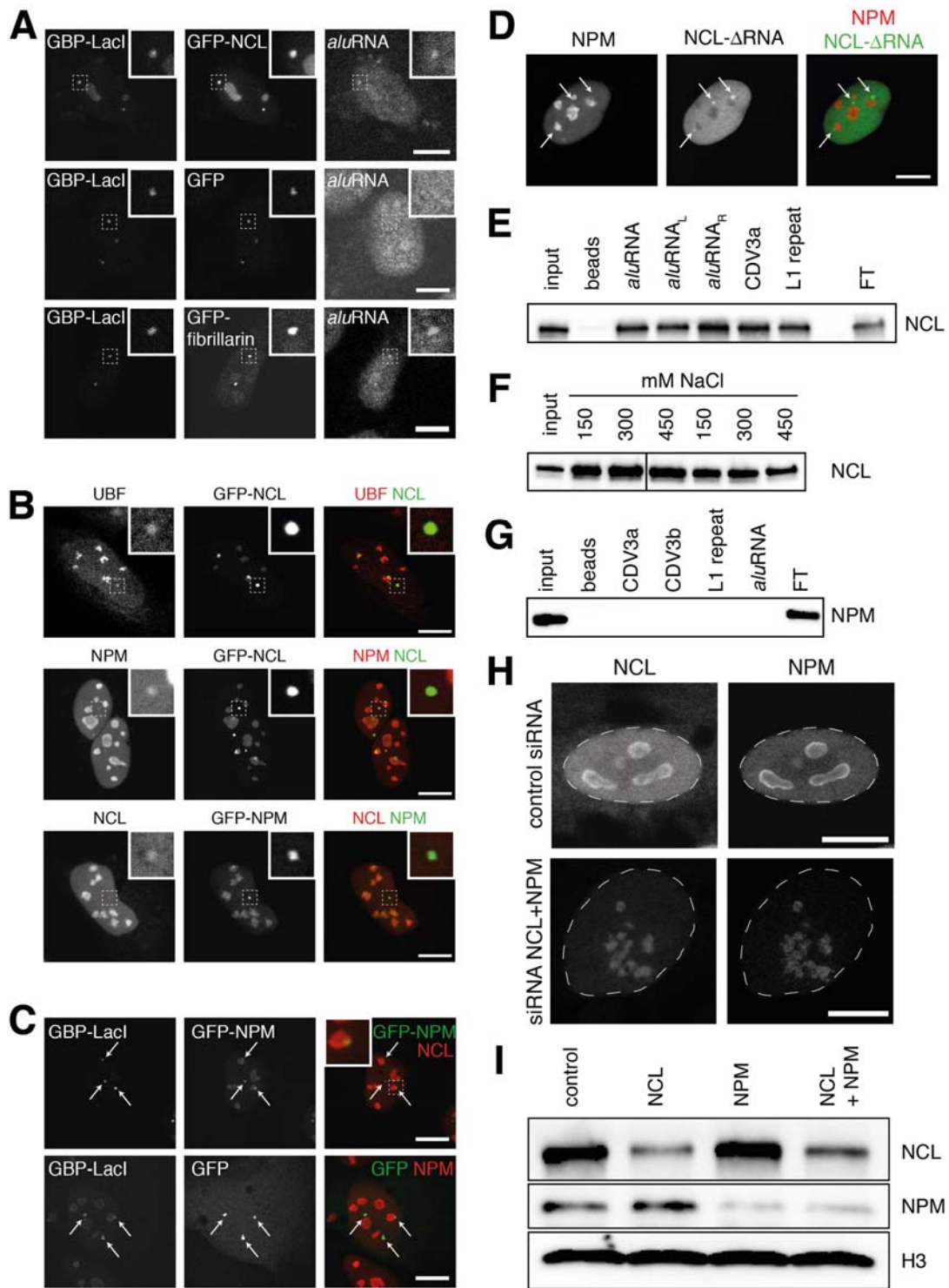
Scale bars, 10  $\mu$ m.



**Appendix Figure S8. Kinetics of nucleoli disruption upon inhibition of Pol II activity by  $\alpha$ -amanitin or depletion of *alu*RNAs are traced by time-lapse imaging.**

CLSM images of HeLa cells under different treatment conditions. Nucleoli were visualized by immunofluorescence of NPM immunostaining, DNA by staining with DAPI. Scale bars in all images, 10  $\mu$ m.

A.  $\alpha$ -amanitin. B. ASO directed against the forward *alu*RNA. C. Blocking LNA probe directed against the forward *alu*RNA sequence. D. Blocking LNA probes directed against L1-repeat RNA.



**Appendix Figure S9. NCL and NPM are required to preserve the nucleolar structure and interact differently with *alu*RNA.**

A-D, H. CLSM images showing the localization of the indicated proteins or RNAs. For recruitment of proteins to *lacO* arrays (panel A-D) the U2OS F6B2 cell line was used. Scale bars, 10  $\mu$ m.

- A. GBP-LacI-RFP, GFP-NCL, GFP or GFP-fibrillarin in comparison to *alu*RNA visualized by RNA FISH. The insets show enlarged images of one of the *lacO* loci.
- B. Immunostained UBF (red) and GFP-NCL (green), immunostained NPM (red) and GFP-NCL (green), or immunostained NCL (red) and GFP-NPM (green). Insets indicate examples of *lacO* arrays to which the GFP-tagged protein was recruited.
- C. GBP-LacI-RFP, GFP-NPM or GFP (green), and NCL or NPM visualized by immunostaining (red). Arrows indicate the stable inserted *lacO* arrays. The inset shows an example of a *lacO* array that is localized in the nucleolus.
- D. NPM (immunofluorescence, red) and GFP-NCL- $\Delta$ RNA (green). Arrows indicate the position of the *lacO* array.
- E-G. Western blot analysis of NCL or NPM binding to RNA in pull-down experiments using nuclear extract and different biotinylated RNA sequences (see also Appendix Table S4). The lane labeled with “beads” indicates a sample that contained only the magnetic beads without biotinylated RNA. FT corresponds to the flow through fraction.
- E. Binding of NCL to different RNAs at a 200 mM concentration of NaCl. 0.7  $\mu$ g/ $\mu$ l nuclear proteins were used. The FT sample is separated from the others by an empty lane.
- F. Salt-dependent binding of NCL to forward *alu*RNA at 70  $\mu$ g (lanes 2-4) and 35  $\mu$ g (lanes 5-7) nuclear protein amount per 100  $\mu$ l reaction volume. Due to a broken well, 2 empty lanes, were removed from the blot image between the 3<sup>rd</sup> and 4<sup>th</sup> lane as marked by the line.
- G. Binding of NPM to indicated RNAs under the same conditions as in panel E.
- H. NCL and NPM distribution in HeLa cells transfected with siRNAs as indicated. Images were taken with the same settings to allow for the comparison of fluorescence signals.
- I. Western blot analysis of siRNA-mediated depletion of NCL and NPM in HeLa cells. Histone H3 was used as loading control. siRNA treatments reduced the amount of the corresponding protein by more than 50% (NCL) and 80% (NPM).